Department für Physik
Ludwig-Maximilians-Universität München

Interferometry in Higher-Dimensional Hilbert Spaces

Yvo Fischer

30. September 2011

Betreut durch Prof. Dr. H. Weinfurter
Zweitgutachter: Prof. Dr. S. Kehrein

Contents

1. Introduction

Quantum mechanics can describe physical systems in accordance to experimental observations that seem counterintuitive from a classical point of view. Also, Einstein, Podolsky, and Rosen (EPR) did not question the correctness of quantum mechanics in their publication titled "Can Quantum-Mechanical Description of Reality Be Considered Complete?" [12] from 1935. But they adressed the philosophical question if the theoretical framework of quantum mechanics can give full knowledge of reality. The example they chose for their argumentation was an entangled quantum mechanical state describing a system itself consisting of two subsystems.

In this work entangled two-photon states were under experimental scrutiny. When measuring the two photons correlations between the results are observed which are covered by quantum mechanics but not by classical physics, or more precisely, they are not covered by the statistics of independent events. A criterion for the decision whether experimentally measured correlations could be explained by such classical statistics was given by Bell [4, 3, 6, 5] three decades after EPR's considerations by defining inequalities. Nowadays the notion "Bell inequality" not only stands for his original inequalities but also for a whole class of similar ones.

Bell inequalities were tested on the experimental setup described in this work. Such Bell tests can verify the nonlocal correlations between the two parties' measurement results and consequently evidence the entanglement of the corresponding quantum mechanical state. This is useful for several applications, e. g. in the field of quantum cryptography where Bell tests can ensure the inherent security of a quantum communication channel [13]. A method of entangling states especially suitable for quantum communication is time-energy entanglement as it is preserved even over long distances [33]. Though, a challenging feature of time-energy entanglement is the requirement for high stability of the used interferometers. This task could be achieved for the experimental setup that this thesis is concerned with [26].

Another property making time-energy entanglement an advantageous choice for quantum communication [34] and quantum computation is its extensibility to higher dimensions [35, 20] enabling the encoding of more information in one pair of entangled photons [25] and the reduction of elemental gates, respectively [24]. Thus, an experimental scheme originally proposed by Franson [16] in 1989

was extended in this experiment. As entanglement in higher dimensions may yield more complex correlations it is reasonable to define Bell inequalities which take them into account [11, 37, 2].

Therefore, the aim of this work was to characterize entangled states defined in higher-dimensional Hilbert spaces by measuring the corresponding interference visibilities and by performing suitable Bell tests.

2. Quantum mechanical description of the experiment

In this chapter the experimental setup is quantum mechanicaly described in a suitable way for the derivation of inequalities that lead to Bell tests. Beforehand a short introduction of important quantum mechanical notations is given.

2.1. Mathematical framework

The Hilbert space

Hilbert spaces [23, 36] serve as the mathematical framework for quantum mechanics. In the bra-ket notation introduced by Paul Dirac a vector in a Hilbert space $\mathcal{H}$ is a *ket* $|\psi\rangle$. A Hilbert space which in quantum mechanics usually is defined over the field $\mathbb{C}$ of the complex numbers is a complete inner product space. The inner or scalar product $\langle\phi|\psi\rangle := (|\phi\rangle, |\psi\rangle)$ defines the norm $\big\||\psi\rangle\big\| := \sqrt{\langle\psi|\psi\rangle}$ which itself defines the metric $d(|\phi\rangle, |\psi\rangle) := \big\||\phi\rangle - |\psi\rangle\big\|$ for $|\phi\rangle, |\psi\rangle \in \mathcal{H}$.

The dual space

The dual space $\mathcal{H}^*$ of a Hilbert space $\mathcal{H}$ over $\mathbb{C}$ consists of all bounded i. e. continuous linear functionals $l\colon \mathcal{H} \to \mathbb{C}$:

$$\mathcal{H}^* := \{\, l\colon \mathcal{H} \to \mathbb{C} \mid l \text{ bounded and linear} \,\}$$

As a Hilbert space $\mathcal{H}$ is canonically isomorphic to its dual space $\mathcal{H}^*$, i. e. there is an antilinear bijective isometry $\mathcal{A}\colon \mathcal{H}^* \to \mathcal{H}$, each $l \in \mathcal{H}^*$ can be uniquely identified with an element of $\mathcal{H}$ itself through the Riesz representation:

$$\forall l \in \mathcal{H}^*\, \exists_1\, |\phi\rangle \in \mathcal{H}\colon l(|\psi\rangle) = (|\phi\rangle, |\psi\rangle) = \langle\phi|\psi\rangle\, \forall\, |\psi\rangle \in \mathcal{H}$$

This justifies the notation as a *bra* $\langle\phi| \in \mathcal{H}^*$ for a dual space element l that is mapped to the element $\mathcal{A}(l) = |\phi\rangle \in \mathcal{H}$ of the Hilbert space itself by the isometric isomorphism $\mathcal{A}$.

Hermitian operators

The Hermitian adjoint $A^\dagger$ of a linear operator $A\colon \mathcal{H} \to \mathcal{H}$ is defined by

$$\langle\psi|A^\dagger|\phi\rangle := \left(|\psi\rangle, A^\dagger|\phi\rangle\right) = \langle\phi|A|\psi\rangle^* \,\forall\, |\phi\rangle, |\psi\rangle \in \mathcal{H}.$$

A is Hermitian, i. e. self-adjoint, if

$$A^\dagger = A.$$

As in this thesis only finite dimensional Hilbert spaces are considered the Hermitian operator A can be decomposed into

$$A = \sum_n \lambda_n P_n$$

according to the spectral theorem where P_n is the orthogonal projection onto the eigenspace corresponding to the eigenvalue $\lambda_n \in \mathbb{R}$ of A.

2.2. States and observables

Probabilities

In quantum mechanics pure physical states are represented by kets with norm 1 and measurable physical properties by Hermitian operators called observables. If a physical state is not pure but a statistical mixture of pure states it cannot be represented by a single vector which itself can be a superposition of pure vectors. Instead, a statistical mixture of – without loss of generality – orthonormal pure states can be described by a density matrix

$$\rho := \sum_k p_k |\psi_k\rangle \langle\psi_k|, \sum_k p_k = 1, \tag{2.1}$$

where p_k is the probability that the system was prepared with in the pure state $|\psi_k\rangle$.

The measurement of a physical property gives an eigenvalue of the corresponding Hermitian operator as result. If the system is in the state ρ the probability of getting the result λ_n for a measurement of the property corresponding to the Hermitian operator $A = \sum_n \lambda_n P_n$ is

$$p(\lambda_n) = \mathrm{Tr}(\rho P_n). \tag{2.2}$$

Entanglement

The Hilbert space $\mathcal{H}$ of a system which consists of two subsystems corresponding to the Hilbert spaces $\mathcal{H}_1$ and $\mathcal{H}_2$ respectively is the tensor product

$$\mathcal{H} = \mathcal{H}_1 \otimes \mathcal{H}_2.$$

The orthonormal basis of the compound system consists of all tensor products

$$|n\rangle \otimes |m\rangle$$

where $|n\rangle$ and $|m\rangle$ are elements of an orthonormal basis of $\mathcal{H}_1$ and $\mathcal{H}_2$, respectively. A state $|\psi\rangle \in \mathcal{H} = \mathcal{H}_1 \otimes \mathcal{H}_2$ which can be decomposed into a tensor product

$$|\psi\rangle = |\psi_1\rangle \otimes |\psi_2\rangle$$

of a state $|\psi_1\rangle \in \mathcal{H}_1$ and a state $|\psi_2\rangle \in \mathcal{H}_2$ is *separable*. If such a decomposition does not exist the state is *entangled*.

2.3. Franson experiment

In this section a brief introduction to the principle of the experiment of time-energy entanglement proposed by Franson [16] is given. Time-energy entanglement serves for preparing the entangled state used in this experiment.

The two parties in the experiment, Alice and Bob, are each provided with one photon of a pair emitted from a two-photon source. For analysis Alice and Bob are equipped with unbalanced interferometers each implementing a time delay of ΔT and an adjustable phase shift $\phi = \phi_\alpha, \phi_\beta$ acquired at its long arm. The detectors $D_{a,+}, D_{a,-}, D_{b,+}, D_{b,-}$, one at each interferometer output, enable Alice and Bob to register the photons (see Figure 2.1). Both photons of a pair are created simultaneously but the absolute time of emission of the photon pair itself is undetermined up to the coherence time $t_{c,\text{creation}}$[22] of its creation process.

Though the beamsplitters distribute with equal probability among their outputs single photon interference of a photon's spatial mode corresponding to the path in the interferometer's long arm with the spatial mode corresponding to the path in the respective short arm is not possible as the photon's coherence time is orders of magnitude smaller than the time delay acquired:

$$t_{c,\text{photon}} \ll \Delta T$$

But the two-photon states encoded for both parties are coherent as

$$\Delta T \ll t_{c,\text{creation}}.$$

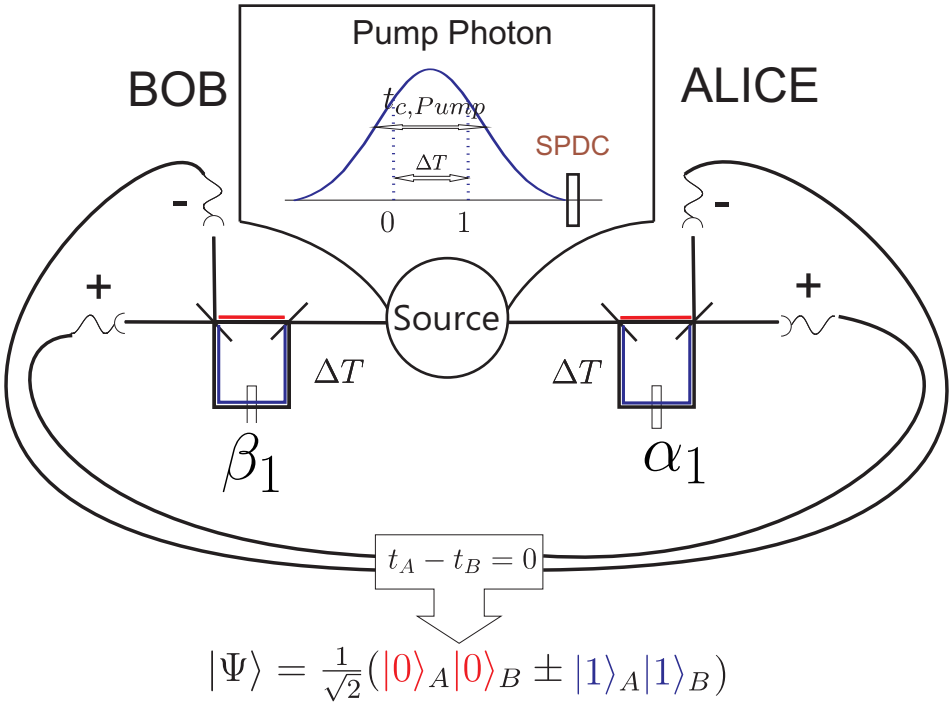

Figure 2.1.: Schematic depiction of the Franson experiment. The source emits pairs of photons. Each interferometer implements a time delay of ΔT and an adjustable phase shift $\phi = \phi_\alpha, \phi_\beta$ for its long arm with respect to its short arm. The beam splitters have a $50:50$ splitting ratio. For coincidences with relative time delay $t_A - t_B = 0$ the entangled state $|\Psi\rangle$ is detected. Each of the two interferometer outputs at Alice's and Bob's side is equipped with a single photon detector labeled "+" or "−" respectively.

In this case Alice and Bob can observe interference of the two-photon state where both photons travel the short arms with the two-photon state where both travel the long arms by triggering on coincidences with equal arrival time for both photons.

Describing each party's interferometer by a two dimensional Hilbert space $\mathcal{H}$ an orthonormal basis is formed by the state $|0\rangle$ corresponding to the short arm and the state $|1\rangle$ corresponding to the long arm. In this notation the two-photon state analyzed by triggering on coincidences with equal arrival time at the detectors $D_{a,+}$ on Alice's and $D_{b,+}$ on Bob's side reads

$$\frac{1}{\sqrt{2}}\left(|0\rangle_a \otimes |0\rangle_b + \mathrm{e}^{\mathrm{i}\phi_\alpha}\,|1\rangle_a \otimes \mathrm{e}^{\mathrm{i}\phi_\beta}\,|1\rangle_b\right) \in \mathcal{H}_a \otimes \mathcal{H}_b \tag{2.3}$$

where the subscripts a and b respectively denote Alice's and Bob's interferometer. This state is entangled because it cannot be rewritten as a tensor product $|x\rangle_a \otimes |y\rangle_b, |x\rangle_a \in \mathcal{H}_a, |y\rangle_b \in \mathcal{H}_b$.

2.4. State from the source

For the experiment considered in this work the interferometer system of the Franson experiment is extended by two additional interferometers, one for Alice and one for Bob. What will be explained in the following about one party's interferometer system applies analogously to the other.

The first interferometer implements a time delay of ΔT for its long arm with respect to its short arm. The delay in the second interferometer is $2\Delta T$ (see Figure 2.2). By transmitting a photon through the short or long arm in the first and the short or long arm in the second interferometer it can acquire the time delay $0\Delta T, 1\Delta T, 2\Delta T$ or $3\Delta T$ with equal probability because the beamsplitters that distribute between the short and the long arm in the interferometers have a $50:50$ splitting ratio (see Table 2.1 on page 12). Computing the delay Δt_{single} of the respective path in the binary system in multiples of ΔT gives an intuitive representation. The digit with subindex 0, i. e. the last digit, corresponds to the first interferometer and the digit with subindex 1 to the second interferometer. This notation becomes advantageous for generalisations to more interferometers and higher dimensions (see Chapter 6). In this case of only two interferometers per party the usual decimal system will be used to describe the two-party system states.

Each path with its specific time delay $\Delta t_{\text{single}} = m\Delta T$ is bijectively mapped to a basis state $|m\rangle, m \in \{0, 1, 2, 3\}$. As the coherence time of the single photon is much shorter than the delay ΔT no single photon interference can

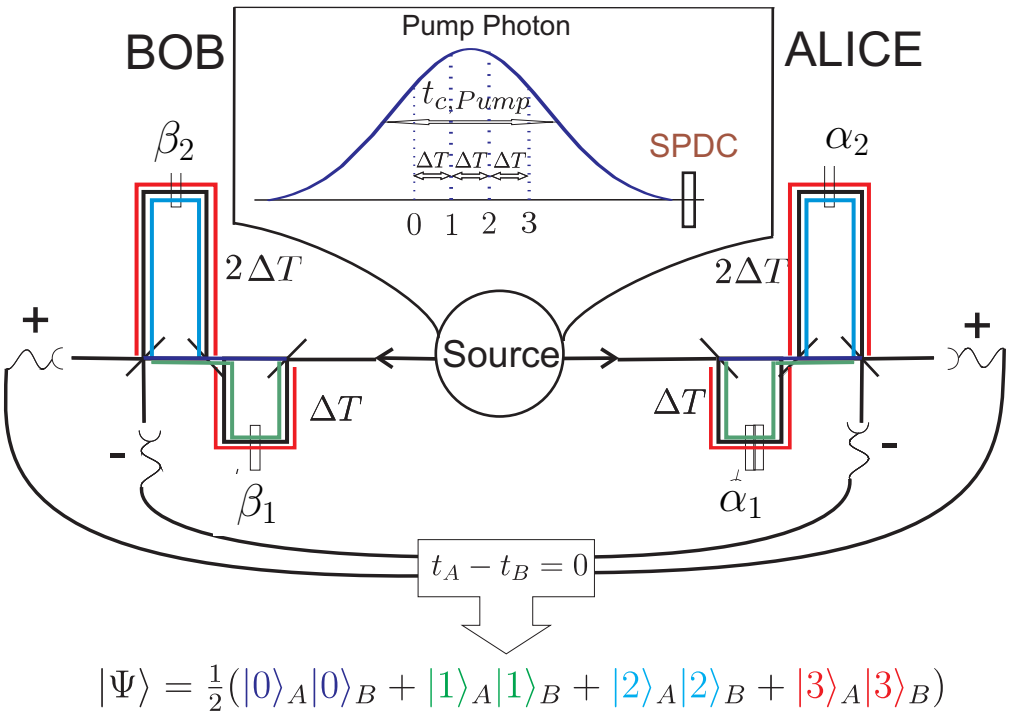

Figure 2.2.: Scheme of the interferometer system used in this experiment for the creation of the four-dimensional time-energy entangled state $|\Psi\rangle$. Phases can be adjusted independently in each interferometer implementing the time delay ΔT and $2\Delta T$ respectively.

Table 2.1.: Delays of possible paths in binary and decimal representation. In the first and second column "0" means "short arm" and "1" means "long arm". Note the correspondence to the third column.

interferometer		total delay	
second ($2\Delta T$)	first ($1\Delta T$)	binary	decimal
0	0	00	0
0	1	01	1
1	0	10	2
1	1	11	3

occur. Hence only two-party states will be under consideration here. The set

$$\{\, |k,l\rangle := |k\rangle|l\rangle := |k\rangle \otimes |l\rangle \mid k,l \in \{0,1,2,3\} \,\}$$

of all tensor products of a basis state $|k\rangle$ for Alice's photon with a basis state $|l\rangle$ for Bob's photon forms a basis for the compound system.

The state of the compound system reads

$$\begin{aligned} |\psi_{\text{source}}\rangle = \ {}^1\!/_4(\quad & |0,0\rangle + |0,1\rangle + |0,2\rangle + |0,3\rangle \\ & + |1,0\rangle + |1,1\rangle + |1,2\rangle + |1,3\rangle \\ & + |2,0\rangle + |2,1\rangle + |2,2\rangle + |2,3\rangle \\ & + |3,0\rangle + |3,1\rangle + |3,2\rangle + |3,3\rangle) \\ \otimes {}^1\!/_2(\quad & |+,+\rangle + |+,-\rangle + |-,+\rangle + |-,-\rangle) \end{aligned} \tag{2.4}$$

where $|a,b\rangle := |a\rangle\,|b\rangle := |a\rangle \otimes |b\rangle$, $a,b \in \{+,-\}$ denotes the outputs a and b where Alice's and respectively Bob's photon are detected. As $|\psi_{\text{source}}\rangle$ is a pure state the corresponding density operator is just the outer product

$$\rho_{\text{source}} \overset{(2.1)}{=} |\psi_{\text{source}}\rangle \langle\psi_{\text{source}}|\,. \tag{2.5}$$

2.5. Analysis of the state

The pairs of entangled photons are produced using the process of spontaneous parametric down-conversion (SPDC) which is described in more detail in chapter A. An important criterion in this experiment is that the time of creation of the pair is undetermined up to the coherence time $t_{c,\text{pump}}$ of the pump photon that is converted into a photon pair in the process. Thus, when the arrival time of a photon at the detector is measured, it is not possible to distinguish whether the photon pair was created $0\Delta T, 1\Delta T, 2\Delta T$ or $3\Delta T$ before the detection[1] because

$$3\Delta T \ll t_{c,\text{pump}}. \tag{2.6}$$

In contrast, the difference Δt_{pair} in the arrival times of the constituents of a pair can in principle be resolved up to their coherence length which is much shorter than ΔT:

$$t_{c,\text{SPDC}} \ll \Delta T \tag{2.7}$$

This, as explained before, renders interference of a single photon's spatial mode $|m\rangle$ with another spatial mode $|n\rangle$ impossible. But inequalities (2.6) and (2.7) give rise to interference of all two-party basis states that share the

[1] Nevertheless no single photon interference can occur. See 2.4.

same acquired time delay Δt_{pair} between Alice's and Bob's photon up to their detection in the same interferometer outputs (see Figure 2.2). Hence, the original state $|\psi_{\text{source}}\rangle$ is projected by coincidence event states

$$|\Delta t_{\text{pair}}, a, b\rangle = \sum_{k-l=\Delta t_{\text{pair}}/\Delta T} c_{k,l,a,b} \, |k, l\rangle \otimes |a, b\rangle \, , c_{k,l,a,b} \in \mathbb{C}$$

where a and b denote the output where Alice's and respectively Bob's photon is registered.

Depending on the output and the path that the prefactor $c_{k,l,a,b}$ corresponds to, it includes additional phase shifts, as the beamsplitters at the interferometer system outputs, like all beamsplitters in the setup, introduce a phase shift of $\pi/2$, i. e. a factor $\mathrm{e}^{\mathrm{i}\pi/2} = \mathrm{i}$, if a photon enters at the "+" or "−" input of the beamsplitter but leaves at the "−" or respectively "+" output [38].

In addition to these phase shifts the photons acquire a phase in the long arm of an interferometer with respect to its short arm. The amount of this relative phase can be adjusted. The relative phases – modulo 2π – acquired in Alice's first and second interferometer are denoted by α_1 and α_2 respectively. Analogously β_1 and β_2 are defined for Bob's interferometers.

There are four output combinations $|+,+\rangle \, , |+,-\rangle \, , |-,+\rangle$ and $|-,-\rangle$. As $k, l \in \{0, 1, 2, 3\}$ implies $\Delta t_{\text{pair}} \in \{-3\Delta T, \ldots, 3\Delta T\}$ there are 7 coincidence windows summing up to $4{\cdot}7 = 28$ distinguishable coincidence events $|\Delta t_{\text{pair}}, a, b\rangle \, , a, b \in \{+1, -1\}$ which are listed in Table 2.2 on page 15. The corresponding projectors $P_{\Delta t_{\text{pair}},a,b}$ can be computed by forming outer products:

$$P_{\Delta t_{\text{pair}},a,b} = |\Delta t_{\text{pair}}, a, b\rangle \, \langle \Delta t_{\text{pair}}, a, b| \tag{2.8}$$

In the following the projected two-photon state $|0\Delta T, +, +\rangle$ serves as an example in order to explain how the phases acquired during the photon's passage through the interferometer system determine the prefactors $c_{k,l,a,b}$ (see Figure 2.2). The state $|0\Delta T, +, +\rangle$ is a superposition of four basis states. The basis state $|0, 0\rangle \otimes |+, +\rangle$ denotes the paths of Alice's and Bob's photon, respectively, that lead through the "+" inputs and the "+" outputs at the respective beam splitters. Therefore none of the paths involves a long interferometer arm. This short two-photon path can be defined to introduce the phases $\phi_a = 0$ for Alice and $\phi_b = 0$ for Bob which serve as the reference for the calculation of the relative phases acquired in other paths, i. e.

$$c_{0,0,+,+} = \mathrm{e}^{\mathrm{i}(0+0)} = 1. \tag{2.9}$$

The second basis state $|1, 1\rangle \otimes |+, +\rangle$ in the superposition $|0\Delta T, +, +\rangle$ denotes the paths where both photons take the long arm in the respective first

Table 2.2.: 28 different projections onto the two-photon states prepared after their passage through the interferometer system paths and their detection at the $+, -$ outputs.

$$|3\Delta T, a, b\rangle = |3, 0\rangle \otimes |a, b\rangle \, , a, b \in \{+, -\}$$

$$|2\Delta T, a, b\rangle = \frac{1}{\sqrt{2}}\left(|2, 0\rangle + \mathrm{e}^{\mathrm{i}(\pi+\alpha_1+\beta_1)} |3, 1\rangle\right) \otimes |a, b\rangle \, , a, b \in \{+, -\}$$

$$|1\Delta T, +, +\rangle = \frac{1}{\sqrt{3}}\left(|1, 0\rangle + \mathrm{e}^{\mathrm{i}(\pi-\alpha_1+\alpha_2+\beta_1)} |2, 1\rangle + \mathrm{e}^{\mathrm{i}(\pi+\alpha_2+\beta_2)} |3, 2\rangle\right) \otimes |+, +\rangle$$

$$|1\Delta T, +, -\rangle = \frac{1}{\sqrt{3}}\left(|1, 0\rangle + \mathrm{e}^{\mathrm{i}(\pi-\alpha_1+\alpha_2+\beta_1)} |2, 1\rangle + \mathrm{e}^{\mathrm{i}(\alpha_2+\beta_2)} |3, 2\rangle\right) \otimes |+, -\rangle$$

$$|1\Delta T, -, +\rangle = \frac{1}{\sqrt{3}}\left(|1, 0\rangle + \mathrm{e}^{\mathrm{i}(-\alpha_1+\alpha_2+\beta_1)} |2, 1\rangle + \mathrm{e}^{\mathrm{i}(\alpha_2+\beta_2)} |3, 2\rangle\right) \otimes |-, +\rangle$$

$$|1\Delta T, -, -\rangle = \frac{1}{\sqrt{3}}\left(|1, 0\rangle + \mathrm{e}^{\mathrm{i}(-\alpha_1+\alpha_2+\beta_1)} |2, 1\rangle + \mathrm{e}^{\mathrm{i}(\pi+\alpha_2+\beta_2)} |3, 2\rangle\right) \otimes |-, -\rangle$$

$$|0\Delta T, \pm, \pm\rangle = \frac{1}{2}\left(|0, 0\rangle + \mathrm{e}^{\mathrm{i}(\alpha_1+\beta_1)} |1, 1\rangle + \mathrm{e}^{\mathrm{i}(\alpha_2+\beta_2)} |2, 2\rangle + \mathrm{e}^{\mathrm{i}(\alpha_1+\alpha_2+\beta_1+\beta_2)} |3, 3\rangle\right) \otimes |\pm, \pm\rangle$$

$$|0\Delta T, \pm, \mp\rangle = \frac{1}{2}\left(|0, 0\rangle + \mathrm{e}^{\mathrm{i}(\alpha_1+\beta_1)} |1, 1\rangle + \mathrm{e}^{\mathrm{i}(\pi+\alpha_2+\beta_2)} |2, 2\rangle + \mathrm{e}^{\mathrm{i}(\pi+\alpha_1+\alpha_2+\beta_1+\beta_2)} |3, 3\rangle\right) \otimes |\pm, \mp\rangle$$

$$|-1\Delta T, +, +\rangle = \frac{1}{\sqrt{3}}\left(|0, 1\rangle + \mathrm{e}^{\mathrm{i}(\pi+\alpha_1-\beta_1+\beta_2)} |1, 2\rangle + \mathrm{e}^{\mathrm{i}(\pi+\alpha_2+\beta_2)} |2, 3\rangle\right) \otimes |+, +\rangle$$

$$|-1\Delta T, +, -\rangle = \frac{1}{\sqrt{3}}\left(|0, 1\rangle + \mathrm{e}^{\mathrm{i}(\alpha_1-\beta_1+\beta_2)} |1, 2\rangle + \mathrm{e}^{\mathrm{i}(\alpha_2+\beta_2)} |2, 3\rangle\right) \otimes |+, -\rangle$$

$$|-1\Delta T, -, +\rangle = \frac{1}{\sqrt{3}}\left(|0, 1\rangle + \mathrm{e}^{\mathrm{i}(\pi+\alpha_1-\beta_1+\beta_2)} |1, 2\rangle + \mathrm{e}^{\mathrm{i}(\alpha_2+\beta_2)} |2, 3\rangle\right) \otimes |-, +\rangle$$

$$|-1\Delta T, -, -\rangle = \frac{1}{\sqrt{3}}\left(|0, 1\rangle + \mathrm{e}^{\mathrm{i}(\alpha_1-\beta_1+\beta_2)} |1, 2\rangle + \mathrm{e}^{\mathrm{i}(\pi+\alpha_2+\beta_2)} |2, 3\rangle\right) \otimes |-, -\rangle$$

$$|-2\Delta T, a, b\rangle = \frac{1}{\sqrt{2}}\left(|0, 2\rangle + \mathrm{e}^{\mathrm{i}(\pi+\alpha_1+\beta_1)} |1, 3\rangle\right) \otimes |a, b\rangle \, , a, b \in \{+, -\}$$

$$|-3\Delta T, a, b\rangle = |0, 3\rangle \otimes |a, b\rangle \, , a, b \in \{+, -\}$$

interferometer. Therefore the phases are shifted by $\pi/2$ twice. First by the change from the "+" input to the "−" output at the respective first beamsplitter and secondly by the change from the "−" input to the "+" output at the second beamsplitter. Additional phases – modulo 2π – (α_1 for Alice's photon and β_1 for Bob's) are acquired in the long arms of the first interferometers with respect to the short arms. Thus, the second basis state with its prefactor reads

$$\begin{aligned} c_{1,1,+,+} \left|1,1\right\rangle \otimes \left|+,+\right\rangle &= \mathrm{e}^{\mathrm{i}(\pi/2+\pi/2+\alpha_1)} \left|1\right\rangle \otimes \mathrm{e}^{\mathrm{i}(\pi/2+\pi/2+\beta_1)} \left|1\right\rangle \otimes \left|+,+\right\rangle \\ &= \mathrm{e}^{\mathrm{i}(\alpha_1+\beta_1)} \left|1,1\right\rangle \otimes \left|+,+\right\rangle . \end{aligned} \tag{2.10}$$

Similar considerations yield

$$c_{2,2,++} = \mathrm{e}^{\mathrm{i}(\alpha_2+\beta_2)}, \tag{2.11}$$

$$c_{3,3,+,+} = \mathrm{e}^{\mathrm{i}(\alpha_1+\alpha_2+\beta_1+\beta_2)}. \tag{2.12}$$

Combining equations (2.10), (2.11), (2.12) and (2.12) the whole superposition reads

$$\begin{aligned} &\left|0\Delta T,+,+\right\rangle = \\ &\frac{1}{2}\big(\left|0,0\right\rangle + \mathrm{e}^{\mathrm{i}(\alpha_1+\beta_1)} \left|1,1\right\rangle + \mathrm{e}^{\mathrm{i}(\alpha_2+\beta_2)} \left|2,2\right\rangle + \mathrm{e}^{\mathrm{i}(\alpha_1+\alpha_2+\beta_1+\beta_2)} \left|3,3\right\rangle\big) \otimes \left|+,+\right\rangle . \end{aligned}$$

2.6. Projector decomposition

Using the described system a projection onto the state $\left|0\Delta T,+,+\right\rangle$ can be performed by selecting the two-photon amplitudes registered in the $\left|+,+\right\rangle$ output combination at time delay $\Delta t_{\mathrm{pair}} = 0$. Though $\left|0,0\right\rangle, \left|1,1\right\rangle, \left|2,2\right\rangle$ and $\left|3,3\right\rangle$ are mutually linearly indepent not the whole four dimensional Hilbert space is spanned by the linear combinations of the form

$$\left|0\Delta T,+,+\right\rangle = \frac{1}{2}\left(\left|0,0\right\rangle + \mathrm{e}^{\mathrm{i}\gamma_1} \left|1,1\right\rangle + \mathrm{e}^{\mathrm{i}\gamma_2} \left|2,2\right\rangle + \mathrm{e}^{\mathrm{i}(\gamma_1+\gamma_2)} \left|3,3\right\rangle\right) \otimes \left|+,+\right\rangle , \tag{2.13}$$

where $\gamma_1 := \alpha_1 + \beta_1$ and $\gamma_2 := \alpha_2 + \beta_2$. Apart from adjustable relative amplitudes three *independent* relative phases would be a necessary condition for reaching – modulo normalization – all points in the four dimensional Hilbert space spanned by

$$\left\{\left|0,0\right\rangle \otimes \left|++\right\rangle, \left|1,1\right\rangle \otimes \left|++\right\rangle, \left|2,2\right\rangle \otimes \left|++\right\rangle, \left|3,3\right\rangle \otimes \left|++\right\rangle\right\}$$

whereas in this case the third relative phase depends on the other two.

In the binary representation from Table 2.1 on page 12 equation (2.13) reads

$$|0\Delta T,+,+\rangle = \tfrac{1}{2}\big(|00,00\rangle + \mathrm{e}^{\mathrm{i}\gamma_1}|01,01\rangle + \mathrm{e}^{\mathrm{i}\gamma_2}|10,10\rangle + \mathrm{e}^{\mathrm{i}(\gamma_1+\gamma_2)}|11,11\rangle\big)\otimes|+,+\rangle$$
$$= \tfrac{1}{2}\big(|00\rangle\otimes|00\rangle + \mathrm{e}^{\mathrm{i}\gamma_1}|01\rangle\otimes|01\rangle + \mathrm{e}^{\mathrm{i}\gamma_2}|10\rangle\otimes|10\rangle + \mathrm{e}^{\mathrm{i}(\gamma_1+\gamma_2)}|11\rangle\otimes|11\rangle\big)\otimes|+,+\rangle\,.$$

The superposing basis states of the four dimensional Hilbert space can be further decomposed by recalling that the single photon basis state $|sf\rangle$, $s,f\in\{0,1\}$, can be seen as a tensor product $|sf\rangle = |s\rangle\otimes|f\rangle$ consisiting of the basis state $|s\rangle$ for the respective second interferometer and the basis state $|f\rangle$ for the respecitve first interferometer. Thus

$$|0\Delta T,+,+\rangle = \tfrac{1}{2}\big(|0\rangle_{a_2}\otimes|0\rangle_{a_1}\otimes|0\rangle_{b_2}\otimes|0\rangle_{b_1} + \mathrm{e}^{\mathrm{i}\gamma_1}|0\rangle_{a_2}\otimes|1\rangle_{a_1}\otimes|0\rangle_{b_2}\otimes|1\rangle_{b_1}$$
$$+\mathrm{e}^{\mathrm{i}\gamma_2}|1\rangle_{a_2}\otimes|0\rangle_{a_1}\otimes|1\rangle_{b_2}\otimes|0\rangle_{b_1} + \mathrm{e}^{\mathrm{i}(\gamma_1+\gamma_2)}|1\rangle_{a_2}\otimes|1\rangle_{a_1}\otimes|1\rangle_{b_2}\otimes|1\rangle_{b_1}\big)\otimes|+,+\rangle$$

where the indices a_1, a_2 denote Alice's first and second interferometer respectively and b_1, b_2 analogously denote Bob's interferometers. By reordering the tensor products it can be shown that the state $|0\Delta T,+,+\rangle$ itself can be represented as a tensor product:

$$|0\Delta T,+,+\rangle = \tfrac{1}{2}\big(|0\rangle_{a_2}\otimes|0\rangle_{b_2}\otimes|0\rangle_{a_1}\otimes|0\rangle_{b_1} + \mathrm{e}^{\mathrm{i}\gamma_1}|0\rangle_{a_2}\otimes|0\rangle_{b_2}\otimes|1\rangle_{a_1}\otimes|1\rangle_{b_1} +$$
$$\mathrm{e}^{\mathrm{i}\gamma_2}|1\rangle_{a_2}\otimes|1\rangle_{b_2}\otimes|0\rangle_{a_1}\otimes|0\rangle_{b_1} + \mathrm{e}^{\mathrm{i}(\gamma_1+\gamma_2)}|1\rangle_{a_2}\otimes|1\rangle_{b_2}\otimes|1\rangle_{a_1}\otimes|1\rangle_{b_1}\big)\otimes|+,+\rangle$$
$$= \frac{1}{\sqrt{2}}\big(|0\rangle_{a_2}\otimes|0\rangle_{b_2} + \mathrm{e}^{\mathrm{i}\gamma_2}|1\rangle_{a_2}\otimes|1\rangle_{b_2}\big)\otimes\frac{1}{\sqrt{2}}\big(|0\rangle_{a_1}\otimes|0\rangle_{b_1} + \mathrm{e}^{\mathrm{i}\gamma_1}|1\rangle_{a_1}\otimes|1\rangle_{b_1}\big)$$
$$\otimes|+,+\rangle$$

Still the state $|0\Delta T,+,+\rangle$ *is* entangled concerning the two-party state distributed to the local entities of Alice's and respectively Bob's interferometer system! The state $|0\Delta T,+,+\rangle$ *cannot* be represented as a tensor product $|a\rangle\otimes|b\rangle$ of a state $|a\rangle$ from the Hilbert space $\mathcal{H}_a$ that corresponds to Alice's interferometer system and a state $|b\rangle$ from the Hilbert space $\mathcal{H}_b$ that corresponds to Bob's interferometer system. Rather the state $|0\Delta T\rangle$ is a tensor product of entangled states each of them being an element of a Hilbert space corresponding to the subsystem of *both* first interferometers and respectively *both* second interferometers (see Figure 2.2). This resembles hyperentanglement where entanglement is observed and exploited in two or more degrees of freedom separately.

2.7. Coincidence functions

In the experiment coincidence count rates can be associated with each projector and serve as a source of information about the detected state. Coincidence

functions, i. e., probabilites which correspond to the 28 distinguishable coincidence events shall be derived in this section.

Moreover the coincidence functions shall be grouped in order to define correlation functions. In this way functions displaying full information about the correlations between both parties can be defined.

Derivation

The relative count rates of the 28 distinguishable coincidence events can be predicted by calculating the corresponding probabilities

$$\begin{aligned} p(\Delta t_{\text{pair}}, a, b) &\overset{(2.2)}{=} \operatorname{Tr}\left(\rho_{\text{source}}\, P_{\Delta t_{\text{pair}},a,b}\right) \\ &\overset{(2.5),(2.8)}{=} \operatorname{Tr}\Big(|\psi_{\text{source}}\rangle \langle\psi_{\text{source}}|\Delta t_{\text{pair}}, a, b\rangle \langle\Delta t_{\text{pair}}, a, b|\Big) \\ &= \langle\psi_{\text{source}}|P_{\Delta t_{\text{pair}},a,b}|\psi_{\text{source}}\rangle \end{aligned}$$

from theory where $|\psi_{\text{source}}\rangle$ is defined in (2.4) on page 13. All probabilities are listed in Table 2.3 on page 19.

Definition of correlation functions

Many of the distinguishable coincidence events have exactly the same dependence on the phases $\alpha_1, \alpha_2, \beta_1$ and β_2. This means that the distribution of outcomes among the elements of such a subset of events is completely random. By adding the count rates of all events belonging to the same subset the latter is considered as an equivalence class and randomness is canceled as far as possible. The sums over coincidence functions with the same phase dependence are listed in Table 2.4 on page 20.

These newly defined probabilities can be further grouped in the sets

$$\begin{gathered} \left\{p_{0\Delta T,x}, p_{0\Delta T,y}, p_{\pm 2\Delta T}\right\}, \\ \left\{p_{\pm 1\Delta T,x}, p_{\pm 1\Delta T,y}, p_{\pm 1\Delta T,w}, p_{\pm 1\Delta T,z}\right\}, \\ \left\{p_{\pm 3\Delta T}\right\}, \end{gathered}$$

each yielding a constant value for the sum of its constituents:

$$\begin{aligned} p_{0\Delta T,x} + p_{0\Delta T,y} + p_{\pm 2\Delta T} &= 1/2 \\ p_{\pm 1\Delta T,x} + p_{\pm 1\Delta T,y} + p_{\pm 1\Delta T,w} + p_{\pm 1\Delta T,z} &= 3/8 \\ p_{\pm 3\Delta T} &= 1/8 \end{aligned} \tag{2.14}$$

Except for the last group which does not depend on the adjustable phases an advantage of this grouping is that it enables the definition of correlation

Table 2.3.: Coincidence probabilities for all 28 distinguishable coincidence events.

$$
\begin{aligned}
p\left(0\Delta T,+,+\right) = p\left(0\Delta T,-,-\right) &= \frac{1}{4}\cos^2\left(\frac{\alpha_1+\beta_1}{2}\right)\cos^2\left(\frac{\alpha_2+\beta_2}{2}\right) \\
p\left(0\Delta T,+,-\right) = p\left(0\Delta T,-,+\right) &= \frac{1}{4}\cos^2\left(\frac{\alpha_1+\beta_1}{2}\right)\sin^2\left(\frac{\alpha_2+\beta_2}{2}\right)
\end{aligned}
$$

$$
\begin{aligned}
&p\left(-1\Delta T,+,+\right) = p\left(1\Delta T,-,-\right) = \\
&\quad\frac{1}{64}\left(3-2\cos\left(\left(\alpha_1-\beta_1\right)-\alpha_2\right)-2\cos\left(\alpha_2+\beta_2\right)+2\cos\left(\left(\alpha_1-\beta_1\right)+\beta_2\right)\right)
\end{aligned}
$$

$$
\begin{aligned}
&p\left(-1\Delta T,-,-\right) = p\left(1\Delta T,+,+\right) = \\
&\quad\frac{1}{64}\left(3+2\cos\left(\left(\alpha_1-\beta_1\right)-\alpha_2\right)-2\cos\left(\alpha_2+\beta_2\right)-2\cos\left(\left(\alpha_1-\beta_1\right)+\beta_2\right)\right)
\end{aligned}
$$

$$
\begin{aligned}
&p\left(-1\Delta T,+,-\right) = p\left(1\Delta T,-,+\right) = \\
&\quad\frac{1}{64}\left(3+2\cos\left(\left(\alpha_1-\beta_1\right)-\alpha_2\right)+2\cos\left(\alpha_2+\beta_2\right)+2\cos\left(\left(\alpha_1-\beta_1\right)+\beta_2\right)\right)
\end{aligned}
$$

$$
\begin{aligned}
&p\left(-1\Delta T,-,+\right) = p\left(1\Delta T,+,-\right) = \\
&\quad\frac{1}{64}\left(3-2\cos\left(\left(\alpha_1-\beta_1\right)-\alpha_2\right)+2\cos\left(\alpha_2+\beta_2\right)-2\cos\left(\left(\alpha_1-\beta_1\right)+\beta_2\right)\right)
\end{aligned}
$$

$$
\begin{aligned}
p\left(-2\Delta T,a,b\right) = p\left(2\Delta T,a,b\right) &= \frac{1}{16}\sin^2\left(\frac{\alpha_1+\beta_1}{2}\right), \quad a,b\in\{+,-\} \\
p\left(-3\Delta T,a,b\right) = p\left(3\Delta T,a,b\right) &= \frac{1}{64}, \quad a,b\in\{+,-\}
\end{aligned}
$$

Table 2.4.: Probabilities summed over coincidence functions with the same phase dependence.

$$p_{0\Delta T,x} := p(0\Delta T,+,+) + p(0\Delta T,-,-) = \frac{1}{2}\cos^2\left(\frac{\alpha_1+\beta_1}{2}\right)\cos^2\left(\frac{\alpha_2+\beta_2}{2}\right)$$

$$p_{0\Delta T,y} := p(0\Delta T,+,-) + p(0\Delta T,-,+) = \frac{1}{2}\cos^2\left(\frac{\alpha_1+\beta_1}{2}\right)\sin^2\left(\frac{\alpha_2+\beta_2}{2}\right)$$

$$p_{\pm 1\Delta T,x} := p(-1\Delta T,+,+) + p(1\Delta T,-,-) = \frac{1}{32}\left(3 - 2\cos\left((\alpha_1-\beta_1)-\alpha_2\right) - 2\cos(\alpha_2+\beta_2) + 2\cos\left((\alpha_1-\beta_1)+\beta_2\right)\right)$$

$$p_{\pm 1\Delta T,y} := p(-1\Delta T,-,-) + p(1\Delta T,+,+) = \frac{1}{32}\left(3 + 2\cos\left((\alpha_1-\beta_1)-\alpha_2\right) - 2\cos(\alpha_2+\beta_2) - 2\cos\left((\alpha_1-\beta_1)+\beta_2\right)\right)$$

$$p_{\pm 1\Delta T,w} := p(-1\Delta T,+,-) + p(1\Delta T,-,+) = \frac{1}{32}\left(3 + 2\cos\left((\alpha_1-\beta_1)-\alpha_2\right) - +2\cos(\alpha_2+\beta_2) + 2\cos\left((\alpha_1-\beta_1)+\beta_2\right)\right)$$

$$p_{\pm 1\Delta T,z} := p(-1\Delta T,-,+) + p(1\Delta T,+,-) = \frac{1}{32}\left(3 - 2\cos\left((\alpha_1-\beta_1)-\alpha_2\right) + 2\cos(\alpha_2+\beta_2) - 2\cos\left((\alpha_1-\beta_1)+\beta_2\right)\right)$$

$$p_{\pm 2\Delta T} := \sum_{\Delta t_{\text{pair}}\in\{-2\Delta T,+2\Delta T\}}\ \sum_{a,b\in\{+,-\}} p(\Delta t_{\text{pair}},a,b) = \frac{1}{2}\sin^2\left(\frac{\alpha_1+\beta_1}{2}\right)$$

$$p_{\pm 3\Delta T} := \sum_{\Delta t_{\text{pair}}\in\{-3\Delta T,+3\Delta T\}}\ \sum_{a,b\in\{+,-\}} p(\Delta t_{\text{pair}},a,b) = \frac{1}{8}$$

functions that can be normalized on – theoretically – constant count rates. This method is adopted in Section 5.2.

There correlation functions defined on the set $\{p_{0\Delta T,x}, p_{0\Delta T,y}, p_{\pm 2\Delta T}\}$ are tested:

$$C_1 = \frac{p_{0\Delta T,x} + p_{0\Delta T,y} - p_{\pm 2\Delta T}}{p_{0\Delta T,x} + p_{0\Delta T,y} + p_{\pm 2\Delta T}} = \cos(\alpha_1 + \beta_1) \tag{2.15}$$

$$\begin{aligned} C_2 &= \frac{p_{0\Delta T,x} - p_{0\Delta T,y} - p_{\pm 2\Delta T}}{p_{0\Delta T,x} + p_{0\Delta T,y} + p_{\pm 2\Delta T}} \\ &= \cos^2\left(\frac{\alpha_1 + \beta_1}{2}\right)\cos(\alpha_2 + \beta_2) - \sin^2\left(\frac{\alpha_1 + \beta_1}{2}\right) \end{aligned} \tag{2.16}$$

C_2 contains information about the phases in all interferometers. C_1 contains no information about the phases in the second interferometers.

3. Bell inequalities

In this chapter Bell inequalities shall be derived which can be tested on the described experimental setup. First an introduction to classical probability theory and classical correlation polytopes is given. They constitute a theoretical framework for Bell-type inequalities. This follows the line as described in [29]. After applying those methods to derive the CHSH [9] inequalities the adaption to a higher number of measurement outcomes is considered. At the end the CGLMP inequalities (Collins, Gisin, Linden, Massar, and Popescu [11]) suited for more than two outcomes are introduced.

3.1. Classical correlations and local hidden variables

Bell inequalities represent constraints on probabilities that are fulfilled by events described by classical probability theory. More precisely, in experiments that Bell inequalities are tested on, the latter would be satisfied if the system's statistics can be reproduced by a local hidden variable (LHV) model.

Experiment with two parties, two settings per party and two outcomes per setting

Consider an experiment like the one originally proposed by Franson [16]. In this setup two parties, Alice and Bob, are provided each with a particle of a two-particle system sharing the same state (see Figure 2.1). Each party can independently choose one out of two measurement settings, i. e. $\alpha \in \{1, 2\}$ for Alice and $\beta \in \{1, 2\}$ for Bob. And for each measurement setting there are two possible outcomes, $A_\alpha, B_\beta \in \{+1, -1\}$.

Joint outcomes

As Alice and Bob share the same state they can define joint outcomes after performing independent measurements on their respective particles. If Alice and Bob have chosen their respective measurement settings $\alpha, \beta \in \{1, 2\}$ then,

as Alice's result A_α as well as Bob's result B_β can take values $+1$ or -1, there exist four possible joint outcomes $(A_\alpha = +1, B_\beta = +1)$, $(A_\alpha = +1, B_\beta = -1)$, $(A_\alpha = -1, B_\beta = +1)$ and $(A_\alpha = -1, B_y = -1)$, i. e. in brief $(1,1)$, $(1,-1)$, $(-1,1)$ and $(-1,-1)$, respectively. A constraint that the probabilities $P(A_\alpha = a, B_\beta = b)$ will satisfy for the outcomes $(A_\alpha = a, B_\beta = b)$, $a, b \in \{-1, +1\}$ is

$$\sum_{a,b\in\{-1,+1\}} P(A_\alpha = a, B_\beta = b) = 1. \tag{3.1}$$

Moreover the probability for the joint detection of two events is trivially non-negative and cannot be greater than the probability of each single event:

$$\begin{aligned} 0 &\leq P(A_\alpha = a, B_\beta = b) && (3.2)\\ P(A_\alpha = a, B_\beta = b) &\leq P(A_\alpha = a) && (3.3)\\ P(A_\alpha = a, B_\beta = b) &\leq P(B_\beta = b) && (3.4) \end{aligned}$$

Furthermore the probability for the event $(A_\alpha = +1 \wedge \overline{B_\beta = +1}) \vee (\overline{A_\alpha = +1} \wedge B_\beta = +1)$, i. e. "either A_α or B_β yields $+1$ but not both", trivially cannot exceed 1. This fact serves as another condition:

$$P(A_\alpha = +1) + P(B_\beta = +1) - P(A_\alpha = +1, B_\beta = +1) \leq 1 \tag{3.5}$$

LHV model

If there exists a set of LHVs which can reproduce the experimental data, additional constraints on the probabilities have to be fulfilled. In an LHV model the probabilities of the individual measurement outcomes for Alice and Bob, respectively, are predetermined by the state emitted from the source and independent of the measurement setting chosen by the respective other party. So a suitable set of local hidden variables, i. e. of single outcome probabilities, would be

$$S_{\text{LHV}} := \{p_{A_1;+1}, p_{A_1;-1}, p_{A_2;+1}, p_{A_2;-1}, p_{B_1;+1}, p_{B_1;-1}, p_{B_2;+1}, p_{B_2;-1}\}$$

where $p_{A_\alpha;a} := P(A_\alpha = a)$ is the probability that Alice's outcome A_α for the measurement with setting α takes value a and $p_{B_\beta;b} := P(B_\beta = b)$ is analogously defined for Bob.

S_{LHV} constitutes of $|S_{\text{LHV}}| = 8$ elements. This number can be reduced by considering the constraint

$$p_{X;+1} + p_{X;-1} = 1,\ X \in \{A_1, A_2, B_1, B_2\} \tag{3.6}$$

any LHV model needs to satisfy because there is always a result, either $+1$ or -1. As (3.6) implies $p_{X;-1} = 1 - p_{X;+1}$ the resulting set

$$S'_{\mathrm{LHV}} := \{p_{A_1}, p_{A_2}, p_{B_1}, p_{B_2}\},$$

where $p_X := p_{X;+1}$, now consists of only 4 variables.

Next, it is possible to define constraints on the probabilities of the joint events. An LHV model is assumed to determine them, too. They can be calculated from the single outcome probabilities. As in this LHV model an event detected by a specific party is independent of the simultaneous event at the other party, the probability $P(A_\alpha = a, B_\beta = b)$ of the joint event is the product of the corresponding single probabilities:

$$P(A_\alpha = a, B_\beta = b) = p_{A_\alpha;a} \cdot p_{B_\beta;b} \tag{3.7}$$

This together with (3.6) sets new constraints, in addition to (3.1), for the probabilities $P(A_\alpha = +1, B_\beta = +1)$, $P(A_\alpha = +1, B_\beta = -1)$, $P(A_\alpha = -1, B_\beta = +1)$ and $P(A_\alpha = -1, B_\beta = -1)$ of joint outcomes that are possible for a chosen set of Alice's and Bob's measurement settings α and β. If, e. g., $P(A_\alpha = +1, B_\beta = +1) = 0$, then $P(A_\alpha = +1, B_\beta = -1) = 0$ or $P(A_\alpha = -1, B_\beta = +1) = 0$ because

$$\begin{aligned} P(A_\alpha = +1, B_\beta = +1) = p_{A_\alpha} \cdot p_{B_\beta} = 0 \implies p_{A_\alpha} = 0 \vee p_{B_\beta} = 0 \implies \\ P(A_\alpha = +1, B_\beta = -1) = p_{A_\alpha} \cdot (1 - p_{B_\beta}) = 0 \vee \\ P(A_\alpha = -1, B_\beta = +1) = (1 - p_{A_\alpha}) \cdot p_{B_\beta} = 0. \end{aligned} \tag{3.8}$$

In contrast, a quantum mechanical system does not need to fulfill this constraint. There is a contradiction e. g. for the coincidence probability corresponding to the entangled state analyzed in the Franson experiment (see (2.3)). This probability is of the form

$$P\left(A_\alpha = +1, B_\beta = +1\right) = \frac{1}{2}\cos^2\left(\phi_\alpha + \phi_\beta\right)$$

where outcome $+1$ or -1 respectively means detection in the detector $D_{x,+}$ or $D_{x,-}, x \in a, b$. This probability vanishes for the phases $\phi_\alpha = \phi_\beta = \frac{\pi}{4}$ whereas

$$P\left(A_\alpha = +1, B_\beta = -1\right) = P\left(A_\alpha = -1, B_\beta = +1\right) = \frac{1}{2}\sin^2\left(\phi_\alpha + \phi_\beta\right)$$

is non-zero in this case in contradiction to (3.8).

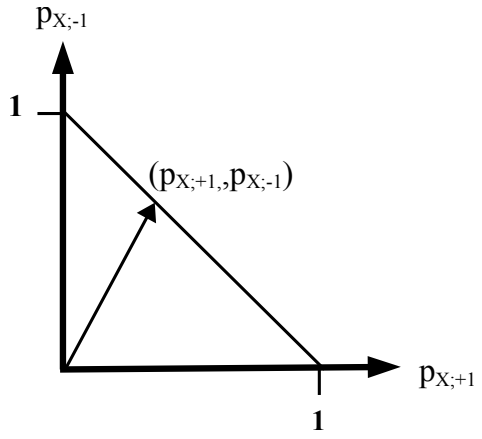

Figure 3.1.: Geometric interpretation of constraint (3.6). The possible values of the vector $(p_{X;+1}, p_{X;-1})$ are constrained to the line segment from $(0,1)$ to $(1,0)$ as $p_{X;+1} + p_{X;-1} = 1$.

3.2. Correlation polytopes and Bell inequalities

What an LHV model is will be further investigated on the basis of the concept of correlation polytopes. Following this framework the CHSH inequalities are derived to give a simple example.

Correlation polytopes

The constraints that were derived in the preceding section have a geometric interpretation. Consider, e. g., within the two dimensional real space the vector $(p_{X;+1}, p_{X;-1})$, whose entries are the probabilites that a measurement of $X \in \{A_1, A_2, B_1, B_2\}$ yields $+1$ and -1, respectively (see Figure 3.1). Constraint (3.6) confines this vector to the diagonal defined by the vertices $(0,1)$ and $(1,0)$. This diagonal is a one dimensional geometric object. So without loss of information, i. e. bijectively, this diagonal can be projected onto the real numbers by mapping

$$(p_{X;+1}, p_{X;-1}) \mapsto$$
$$(+1) \cdot p_{X;+1} + (-1) \cdot p_{X;-1} \overset{(3.6)}{=} (+1) \cdot p_{X;+1} + (-1) \cdot (1 - p_{X;+1}) = 2p_{X;+1} - 1.$$

The image of this mapping is the interval $[-1; +1]$. Later a similar mapping will be defined as a correlation.

Now consider the three dimensional real space and within it the vector $\big(P(A_\alpha = +1), P(B_\beta = +1), P(A_\alpha = +1, B_\beta = +1)\big)$ consisting of the prob-

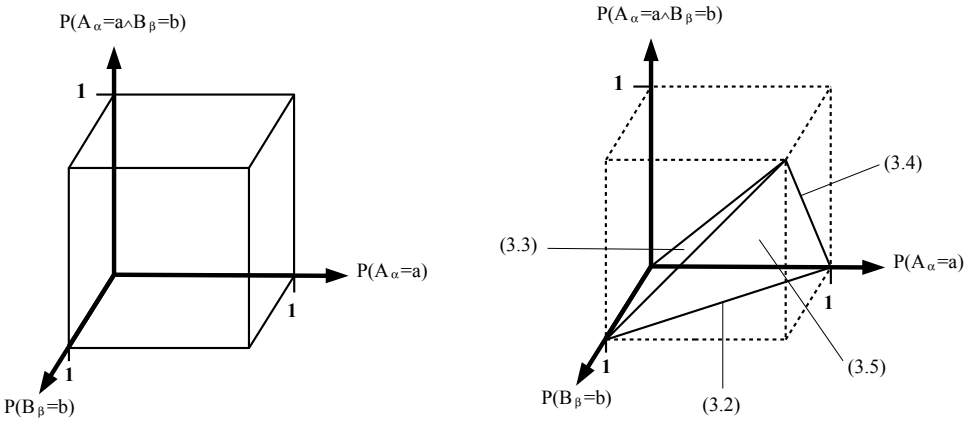

Figure 3.2.: Geometric interpretation of additional constraints. All probabilities are trivially bounded between 0 and 1 (3.2a). Requiring in addition that the probabilities satisfy constraints (3.2), (3.3), (3.4) and (3.5) gives a polytope of smaller volume (3.2b).

abilities $P(A_\alpha = +1)$ and $P(B_\beta = +1)$ for outcome $+1$ in Alice's and Bob's measurement with setting α and β respectively and the probability $P(A_\alpha = +1, B_\beta = +1)$ for the conjunction of those events. As all probabilities are constrained within $[0; 1]$ the vector lies in the cube defined by the vertices $(0, 0, 0)$, $(1, 0, 0)$, $(0, 1, 0)$, $(1, 1, 0)$, $(0, 0, 1)$, $(1, 0, 1)$, $(0, 1, 1)$ and $(1, 1, 1)$ representing its corners (see Figure 3.2a).

In this case constraint (3.6) cannot be applied as the events $(A_\alpha = +1)$ and $(B_\beta = +1)$ don't exclude each other. However, by considering constraints (3.2), (3.3), (3.4) and (3.5) the set of values the vector

$$\big(P(A_\alpha = +1), P(B_\beta = +1), P(A_\alpha = +1, B_\beta = +1)\big)$$

can reach is further limited (see Figure 3.2b). The generated geometrical object, like the cube in Figure 3.2a, is the closed convex hull of its vertices but of smaller volume and with only four delimiting facets. Each of them corresponds to one of the four constraints (3.2), (3.3), (3.4) and (3.5) if "$\leq$" is replaced by "=". In a space of dimension d each of these equations defines, in the manner as constraint (3.6) does, a $(d-1)$ dimensional geometrical object, i. e. a hyperplane.

Table 3.1.: Truth table for the Clauser-Horne polytope. The eight colored row vectors define the hyperplane that corresponds to one of the Clauser-Horne inequalities.

p_{A_1}	p_{A_2}	p_{B_1}	p_{B_2}	p_{A_1,B_1}	p_{A_1,B_2}	p_{A_2,B_1}	p_{A_2,B_2}
0	0	0	0	0	0	0	0
0	0	0	1	0	0	0	0
0	0	1	0	0	0	0	0
0	0	1	1	0	0	0	0
0	1	0	0	0	0	0	0
0	1	0	1	0	0	0	1
0	1	1	0	0	0	1	0
0	1	1	1	0	0	1	1
1	0	0	0	0	0	0	0
1	0	0	1	0	1	0	0
1	0	1	0	1	0	0	0
1	0	1	1	1	1	0	0
1	1	0	0	0	0	0	0
1	1	0	1	0	1	0	1
1	1	1	0	1	0	1	0
1	1	1	1	1	1	1	1

From correlation polytopes to inequalities

As it was shown in the preceding paragraphs, following the Weyl-Minkowski theorem[17] the correlation polytope can be described either by its vertices or by equations representing its facets. These equations can in principle be derived once the vertices are known. The latter are calculated by constructing a truth table (see Table 3.1 on page 28). It consists of rows each corresponding to a vertex of the correlation polytope. Each row represents a possible combination to assign truth values 0 and 1 to the single events. Also, each row contains the truth values of the relevant joint events which can be calculated from the row's single event values.

Once the truth table is known it is straightforward to compute the equations describing the facets of the polytope. A hyperplane in a d dimensional space can be defined by d distinct points lying in the hyperplane. So each set of d distinct vertices describes the hyperplane containing the set. The actual computation can be realized by the application of Cramer's rule.

As a prerequisite let $M \in \mathbb{R}^{d\times d}$ denote the matrix that consists of d rows, i. e. vertices, of the d columned truth table. Let $\mathbf{n} = (n_1, \ldots, n_d) \in \mathbb{R}^d$ denote

the in general unnormalized normal vector to the hyperplane. Then n can be derived by solving the system

$$M\mathbf{n}^T = r\underbrace{(1,\ldots,1)}_{d}{}^T \tag{3.9}$$

of linear equations where $r \in \mathbb{R}$ defines the distance $\frac{r}{|\mathbf{n}|}$ between the hyperplane and the origin. If separately read for each row in M, (3.9) states that the projection of the corresponding vertex onto the normal vector $\mathbf{n}$ yields r. This is a sufficient condition for the vertex to lie in the hyperplane.

If none of the rows of M is the null vector then Cramer's rule states

$$\frac{n_j}{r} = \frac{\det(M_j)}{\det(M)}, \quad j = 1,\ldots,d$$

where M_j is the matrix formed by replacing the jth column of M by $(1,\ldots,1)^T$.

If a row of M is the null vector then r equals zero and

$$n_j = (-1)^j \det(M_{0j}), \quad j = 1,\ldots,d$$

holds where $M_{0j} \in \mathbb{R}^{(d-1)\times(d-1)}$ is the Matrix formed by dropping the jth column of M as well as the row which is the null vector.

Applying this method to the matrix $M_{\mathrm{CH},1}$ formed by the eight row vectors marked in Table 3.1 on page 28 yields the normal vector

$$\mathbf{n}_{\mathrm{CH},1} = (-1,0,-1,0,1,1,1,-1).$$

As one of the rows in $M_{\mathrm{CH},1}$ is the null vector, $r_{\mathrm{CH},1}$ vanishes and

$$r_{\mathrm{CH},1} = \mathbf{m}_{\mathrm{CH},1}\mathbf{n}_{\mathrm{CH}}^T = 0 \tag{3.10}$$

holds for any row vector from $M_{\mathrm{CH},1}$. Repeating the procedure for the matrix $M_{\mathrm{CH},2}$ formed by the remaining eight row vectors yields the same normal vector $\mathbf{n}_{\mathrm{CH},2} = \mathbf{n}_{\mathrm{CH},1} =: \mathbf{n}_{\mathrm{CH}}$. In this case, as $M_{\mathrm{CH},2}$ doesn't include the null vector, $r_{\mathrm{CH},2}$ is not zero. The product of any row vector $\mathbf{m}_{\mathrm{CH},2}$ of $M_{\mathrm{CH},2}$ with the normal vector gives

$$r_{\mathrm{CH},2} = \mathbf{m}_{\mathrm{CH},2}\mathbf{n}_{\mathrm{CH}}^T = -1. \tag{3.11}$$

As all row vectors from Table 3.1 on page 28, i. e. all vertices of the Clauser-Horne polytope, satisfy either (3.10) or (3.11) and as the Clauser-Horne polytope is the set of all convex combinations of these vertices, the following inequality holds for all vectors

$$\mathbf{p} = (p_{A_1}, p_{A_2}, p_{B_1}, p_{B_2}, p_{A_1,B_1}, p_{A_1,B_2}, p_{A_2,B_1}, p_{A_2,B_2})$$

that lie inside the Clauser-Horne polytope:

$$\underset{\overset{(3.11)}{=}\mathbf{m}_{\mathrm{CH},2}\mathbf{n}_{\mathrm{CH}}^T}{-1} \leq \underbrace{p_{A_1,B_2} + p_{A_1,B_1} + p_{A_2,B_1} - p_{A_2,B_2} - p_{A_1} - p_{B_1}}_{=\mathbf{p}\mathbf{n}_{\mathrm{CH}}^T} \leq \underset{\overset{(3.10)}{=}\mathbf{m}_{\mathrm{CH},1}\mathbf{n}_{\mathrm{CH}}^T}{0} \tag{3.12}$$

This Bell type inequality is one of the four Clauser-Horne inequalities [8] and it is fulfilled by all row vectors listed in Table 3.1 on page 28.

Number of hyperplanes

If there are k independent single events considered then there are 2^k distinct possibilities to assign the values 0 and 1 to them, i. e. 2^k rows in the corresponding truth table. In the Clauser-Horne (CH [8]) example there are $k = 4$ independent single events of interest resulting in

$$2^k = 2^4 = 16 \tag{3.13}$$

rows (see Table 3.1 on page 28). As there are $l = 4$ joint events of interest the dimension of the real space that contains the Clauser-Horne polytope is

$$d = k + l = 8. \tag{3.14}$$

As a hyperplane in a d dimensional space is defined by d distinct points the number of equations each describing a hyperplane intersecting the Clauser-Horne polytope is

$$\binom{2^k}{\underbrace{k+l}_{=d}} \overset{(3.13),(3.14)}{=} \binom{16}{8} = 12870.$$

This number is much greater than the number of inequalities that are necessary and sufficient to describe the Clauser-Horne polytope:

$$\begin{aligned} &0 \leq p_{A_i,B_j} \leq p_{A_i} \leq 1, \quad 0 \leq p_{A_i,B_j} \leq p_{B_j} \leq 1 && i,j = 1,2 \\ &p_{A_i} + p_{B_j} - p_{A_i,B_j} \leq 1 && i,j = 1,2 \end{aligned}$$

$$\begin{array}{rrrrrrr} -1 \leq & p_{A_1,B_1} & +p_{A_1,B_2} & +p_{A_2,B_2} & -p_{A_2,B_1} & -p_{A_1} & -p_{B_2} & \leq 0 \\ -1 \leq & p_{A_2,B_1} & +p_{A_2,B_2} & +p_{A_1,B_2} & -p_{A_1,B_1} & -p_{A_2} & -p_{B_2} & \leq 0 \\ -1 \leq & p_{A_1,B_2} & +p_{A_1,B_1} & +p_{A_2,B_1} & -p_{A_2,B_2} & -p_{A_1} & -p_{B_1} & \leq 0 \\ -1 \leq & p_{A_2,B_2} & +p_{A_2,B_1} & +p_{A_1,B_1} & -p_{A_1,B_2} & -p_{A_2} & -p_{B_1} & \leq 0 \end{array}$$

These are 36 inequalities in total if each "$\leq$"-relation and index combination (i, j) is counted seperately.[1] The last four inequalities – eight inequalities, if each "$\leq$" is counted separately – are called Clauser-Horne inequalities. They are formally equivalent to the CHSH inequality. The latter is introduced at the end of this section as it is experimentally better accessible.

Bounds of expressions

The preceding example shows that it is important to distinguish the hyperplanes that delimit i. e. touch the polytope from the ones that merely intersect it, especially if d and consequently the number of hyperplanes is increased. In order to decide if a hyperplane described by its normal vector n and its distance $\frac{r}{|n|}$ from the origin delimits the correlation polytope it can be tested if r is an extremal value of the expression

$$pn = (p_1, \ldots, p_d) \begin{pmatrix} n_1 \\ \vdots \\ n_d \end{pmatrix} \tag{3.15}$$

for every p being an element of the correlation polytope. As each such p is a finite convex combination

$$p = \sum_{i=1}^{2^k} c_i \cdot v_i, \quad \sum_{i=1}^{2^k} c_i = 1, c_i \geq 0$$

of the polytope's vertices v_i, each corresponding to a row vector of the truth table, it is sufficient to check if either

$$v_i n \leq r \quad \forall i = 1, \ldots, 2^k$$

or

$$v_i n \geq r \quad \forall i = 1, \ldots, 2^k$$

in order to test the extremality of 3.15.

CHSH

The CHSH inequality

$$-2 \leq C(A_1, B_1) - C(A_1, B_2) + C(A_2, B_1) + C(A_2, B_2) \leq 2, \tag{3.16}$$

[1] According to Collins and Gisin [10] "(t)here is no need for inequalities stating that probabilities should be not greater than 1, since this follows from all the probabilities being positive."

where

$$C(A_\alpha, B_\beta) = P(A_\alpha = +1, B_\beta = +1) - P(A_\alpha = +1, B_\beta = -1) \quad (3.17)$$
$$-P(A_\alpha = -1, B_\beta = +1) + P(A_\alpha = -1, B_\beta = -1) \quad (3.18)$$

is a correlation function, is equivalent to one of the derived Clauser-Horne inequalities [32]. By rewriting (3.17) as

$$\begin{aligned} C(A_\alpha, B_\beta) &= 4P(A_\alpha = +1, B_\beta = +1) \\ &\quad -2\big(P(A_\alpha = +1, B_\beta = +1) + P(A_\alpha = +1, B_\beta = -1)\big) \\ &\quad -2\big(P(A_\alpha = +1, B_\beta = +1) + P(A_\alpha = -1, B_\beta = +1)\big) \\ &\quad +\big(P(A_\alpha = +1, B_\beta = +1) + P(A_\alpha = +1, B_\beta = -1) \\ &\quad +P(A_\alpha = -1, B_\beta = +1) + P(A_\alpha = -1, B_\beta = -1)\big) \\ &= 4P(A_\alpha = +1, B_\beta = +1) - 2P(A_\alpha = +1) - 2P(B_\beta = +1) + 1 \end{aligned}$$

and substituting it into (3.16) one gets

$$\begin{aligned} -2 \leq\ & 4P(A_1 = +1, B_1 = +1) - 4P(A_1 = +1, B_2 = +1) \\ & + 4P(A_2 = +1, B_1 = +1) + 4P(A_2 = +1, B_2 = +1) \\ & - 4P(A_2 = +1) - 4P(B_1 = +1) + 2 \leq 2. \end{aligned}$$

After subtraction of 2 and subsequent division by 4 it yields the CH inequality

$$\begin{aligned} -1 \leq\ & P(A_1 = +1, B_1 = +1) - P(A_1 = +1, B_2 = +1) \\ & + P(A_2 = +1, B_1 = +1) + P(A_2 = +1, B_2 = +1) \\ & - P(A_2 = +1) - P(B_1 = +1) \leq 0. \end{aligned}$$

The CHSH inequality can be tested on the states experimentally prepared in this work. This will be undertaken concerning the states detected as coincidences with relative time delay $0\Delta T$ and $\pm 2\Delta T$ in Chapter 5. There, sets of numerically optimized angles are listed that yield a maximum quantum value of $2\sqrt{2}$ for the CHSH expression.

3.3. Bell inequalities for higher dimensional systems

In the last section it was shown how an LHV model constrains the probabilities of joint measurement outcomes. Those conditions were interpreted geometrically as the supporting hyperplanes of a correlation polytope. A straightforward method was introduced for calculating the inequalities each corresponding to a specific hyperplane of the polytope. The task of the distinction of the

relevant inequalities from a possible multitude of trivial ones arises, similar to the CH inequalities, for higher-dimensional systems. A task similar to the distinction of the delimiting from the intersecting hyperplanes of the Clauser-Horne polytope arises for higher-dimensional systems, as the distinction of the relevant inequalities from a possible multitude of trivial inequalities is not straightforward.

CGLMP inequalities

In their article "Bell Inequalities for Arbitrarily High-Dimensional Systems" Collins, Gisin, Linden, Massar, and Popescu [11] (CGLMP) derive the formula for a class of Bell inequalities for two-party states each defined on a higher-dimensional Hilbert space. As before these inequalities exploit the fact that correlations exhibited by local variable theories must satisfy certain constraints. Such an inequality is tested on the experimentally prepared two-party states in Section 5.1. The most important steps of the CGLMP approach are explained in the following.

In their article CGLMP consider a system with two parties, Alice and Bob, each of them being able to independently choose one out of two distinct measurements A_1, A_2 and respectively B_1, B_2 on a shared higher dimensional state. Each of those measurements yields one of d possible outcomes $A_1, A_2, B_1, B_2 = 0, \ldots, d-1$. In a local variable theory Alice's measurement yields $A_1 = j$ or $A_2 = k$ and Bob's measurement $B_1 = l$ or $B_2 = m$ with probability c_{jklm}, $j, k, l, m \in \{0, \ldots, d-1\}$. Consequently, there are d^4 probabilities c_{jklm} that satisfy $\sum_{jklm} c_{jklm} = 1$ and completely describe the system in a model of local variables (j, k) for Alice and (l, m) for Bob.

For a particular choice $jklm$ of local variables the differences of outcomes can be defined as

$$\begin{aligned} r :=& B_1 - A_1 = l - j, \\ s :=& A_2 - B_1 = k - l, \\ t :=& B_2 - A_2 = m - k, \\ u :=& A_1 - B_2 = j - m. \end{aligned}$$

Three of these differences can be freely chosen but the fourth is constrained since

$$r + s + t + u = (l - j) + (k - l) + (m - k) + (j - m) = 0. \tag{3.19}$$

This constraint is exploited by constructing Bell expressions which involve probabilities $Q(A_a = B_b + n)$ that Alice's and Bob's outcome differ, modulo

d, by n:

$$Q(A_a = B_b + n) := \sum_{i=0}^{d-1} P\left(A_a = i, B_b = (i+n) \bmod d\right) \tag{3.20}$$

The Bell expressions constructed from these probabilities only achieve their maximum value if constraint (3.19) is violated. The simplest such Bell expression is

$$I := Q(A_1 = B_1) + Q(B_1 = A_2 + 1) + Q(A_2 = B_2) + Q(B_2 = A_1)$$

which in the case of two dimensional systems is equivalent to the CHSH inequality (see Section 3.2).

The generalisation to d-dimensional systems introduced by CGLMP for any $d \geq 2$ reads

$$\begin{aligned} I_d := \sum_{n=0}^{[d/2]-1} \left(1 - \frac{2n}{d-1}\right) \Big\{ + \big[& Q\left(A_1 = B_1 + n\right) + Q\left(B_1 = A_2 + n + 1\right) + \\ & Q\left(A_2 = B_2 + n\right) + Q\left(B_2 = A_1 + n\right)\big] - \\ \big[& Q\left(A_1 = B_1 - n - 1\right) + Q\left(B_1 = A_2 - n\right) + \\ & Q\left(A_2 = B_2 - n - 1\right) + Q\left(B_2 = A_1 - n - 1\right)\big] \Big\}. \end{aligned} \tag{3.21}$$

One of the expressions tested in Section 5.1 is

$$\begin{aligned} I_3 = & + \big[Q(A_1 = B_1) \quad + Q(B_1 = A_2 + 1) + Q(A_2 = B_2) \quad + Q(B_2 = A_1)\big] \\ & - \big[Q(A_1 = B_1 - 1) + Q(B_1 = A_2) \quad + Q(A_2 = B_2 - 1) + Q(B_2 = A_1 - 1)\big] \end{aligned} \tag{3.22}$$

The maximum value attainable by local variable theories is independent of d:

$$\max_{\text{local variable}} (I_d) = 2 \quad \forall d \geq 2$$

Output projectors

The class of CGLMP inequalities is defined by sums of probabilities $P(A_\alpha = a, B_\beta = b)$ for joint events. But not all of these events are separately accessible in the described experiment. The joint events $A_\alpha = 0 \wedge B_\beta = 0, A_\alpha = 1 \wedge B_\beta = 1, A_\alpha = 2 \wedge B_\beta = 2$ and $A_\alpha = 3 \wedge B_\beta = 3$ for example cannot be distinguished because they all lead to a $0\Delta T$ coincidence. The same applies to the $\pm 1\Delta T$ and $\pm 2\Delta T$ coincidences.

This problem can be solved by a change of basis. For the Hilbert space e. g. spanned by $\{|0,0\rangle, |1,1\rangle, |2,2\rangle, |3,3\rangle\}$ an alternative orthonormal basis would be the set consisting of

$$\begin{aligned}
|\Psi_0\rangle &:= 1/2\big(|0,0\rangle + |1,1\rangle + |2,2\rangle + |3,3\rangle\big),\\
|\Psi_1\rangle &:= 1/2\big(|0,0\rangle - |1,1\rangle - |2,2\rangle + |3,3\rangle\big),\\
|\Psi_2\rangle &:= 1/2\big(|0,0\rangle - |1,1\rangle + |2,2\rangle - |3,3\rangle\big),\\
|\Psi_3\rangle &:= 1/2\big(|0,0\rangle + |1,1\rangle - |2,2\rangle - |3,3\rangle\big).
\end{aligned}$$

Each projector corresponding to one of these new basis states can be realized by accordingly adjusting the phases $\alpha_1, \alpha_2, \beta_1, \beta_2$, resulting in

$$|0\Delta T, +, +\rangle = 1/2\big(|0,0\rangle + \mathrm{e}^{\mathrm{i}(\alpha_1+\beta_1)}\,|1,1\rangle + \mathrm{e}^{\mathrm{i}(\alpha_2+\beta_2)}\,|2,2\rangle + \mathrm{e}^{\mathrm{i}(\alpha_1+\beta_1+\alpha_2+\beta_2)}\,|3,3\rangle\big).$$

This method, i. e. to measure only "+, +" results, resembles the implementation of a Bell test where the polarization of the photons for a specific analysis setting (α, β) is analyzed in subsequent measurements. In each of them a projection on *one* possible outcome $(A_\alpha = a, B_\beta = b)$ is realized by accordingly adjusted polarizers rather than analyzing the polarization by the application of polarizing beam splitters where *all* outcomes for a specific analysis setting could occur in the same measurement.

A similar change of basis as for the compound system can be separately performed for the Hilbert spaces $\mathcal{H}_a$ and $\mathcal{H}_b$ of Alice and Bob, respectively. The new basis states for a single Hilbert space can be defined in terms of the old basis as

$$\begin{aligned}
|\psi_0\rangle &:= 1/2\big(|0\rangle + |1\rangle + |2\rangle + |3\rangle\big),\\
|\psi_1\rangle &:= 1/2\big(|0\rangle - |1\rangle - |2\rangle + |3\rangle\big),\\
|\psi_2\rangle &:= 1/2\big(|0\rangle - |1\rangle + |2\rangle - |3\rangle\big),\\
|\psi_3\rangle &:= 1/2\big(|0\rangle + |1\rangle - |2\rangle - |3\rangle\big),
\end{aligned}$$

each corresponding to a different output of that single party's analysis apparatus. As before they can be implemented for the "+" detector by accordingly adjusting the phases γ_1', γ_2', resulting in

$$|\psi\rangle := 1/2\big(|0\rangle + \mathrm{e}^{\mathrm{i}\gamma_1'}\,|1\rangle + \mathrm{e}^{\mathrm{i}\gamma_2'}\,|2\rangle + \mathrm{e}^{\mathrm{i}\left(\gamma_1'+\gamma_2'\right)}\,|3\rangle\big).$$

In this framework the detection of a coincidence with no relative time delay in a specific output combination corresponds to a projection of the prepared state onto the tensor product of Alice's and Bob's output projectors denoted by the indices i and j, respectively. The associated probability is

$$\mathrm{Tr}\Big(\Big(\big(|\psi_i\rangle\,\langle\psi_i|\big) \otimes \big(|\psi_j\rangle\,\langle\psi_j|\big)\Big)\rho''_{0\Delta T}\Big).$$

The phases γ_1 and γ_2 adjusted in a party's respective short and long interferometer are the sums of the respective projector and preparation phases:

$$\gamma_i = \gamma_i' + \gamma_i'', i = 1, 2 \tag{3.23}$$

A numerical optimization of the CGLMP expression I_4 over all preparation phases gives a maximum quantum mechanical prediction of

$$\max_{\text{QM}}(I_4) = 2.55 > 2 = \max_{\text{local variable}}(I_4).$$

A set of optimal preparation phases is described in Section 5.1.

4. Experimental scheme and test of the setup

In this chapter the actual implementation of the experimental setup is described. For more details the reader is referred to [26] and [30].

4.1. Source of entangled photons

The source of entangled photons consists of a diode laser[1] which pumps a down-conversion crystal. The laser diode is operated at 402.8 nm and offers a coherence time $t_{c,\mathrm{pump}} = 2.58\,\mu\mathrm{s} \gg \Delta T$ by using an external grating stabilization scheme. The Hänsch-Couillaud[18] locking scheme is applied to fix the central lasing frequency.

A fraction of $\approx 10^{-6}$ of the pump photons is down-converted into a pair of entangled photons in a periodically poled $KTiOPO_4$ (PPKTP) [15, 28] crystal with a poling period of 9.67 µm. For details concerning the theory of the SPDC process see appendix Chapter A.

The wavelength of the down-conversion photons depends on the temperature of the PPKTP crystal. Thus it is placed inside an oven where the temperature is kept at $(26.0 \pm 0.2)\,^{\circ}\mathrm{C}$ in order to ensure the degeneracy of the wavelengths of each photon pair.

The SPDC efficiency η, i. e. the quotient of coincidence count rate and pump power, remains close to $\eta \approx 49 \times 10^3\,(\mathrm{s}\cdot\mathrm{mW})^{-1}$ over a wide range of the pump power. The photons are produced with a central wavelength of $\lambda_{\mathrm{SPDC}} = 805.9\,\mathrm{nm}$ and a bandwidth of $\Delta\lambda_{\mathrm{SPDC}} < 1.1\,\mathrm{nm}$ (see Figure 4.1).

As the down-conversion photons of a pair have orthogonal polarization with respect to each other they can be separated by a polarizing beam splitter (PBS) and be coupled into a single mode fibers each guiding the beam to Alice's and Bob's interferometer system, respectively. This method has the advantage that the probability of feeding both photons of a pair into the same interferometer system is close to zero. Hereby additional loss of coincidences is avoided.

[1] manufactured by Nichia

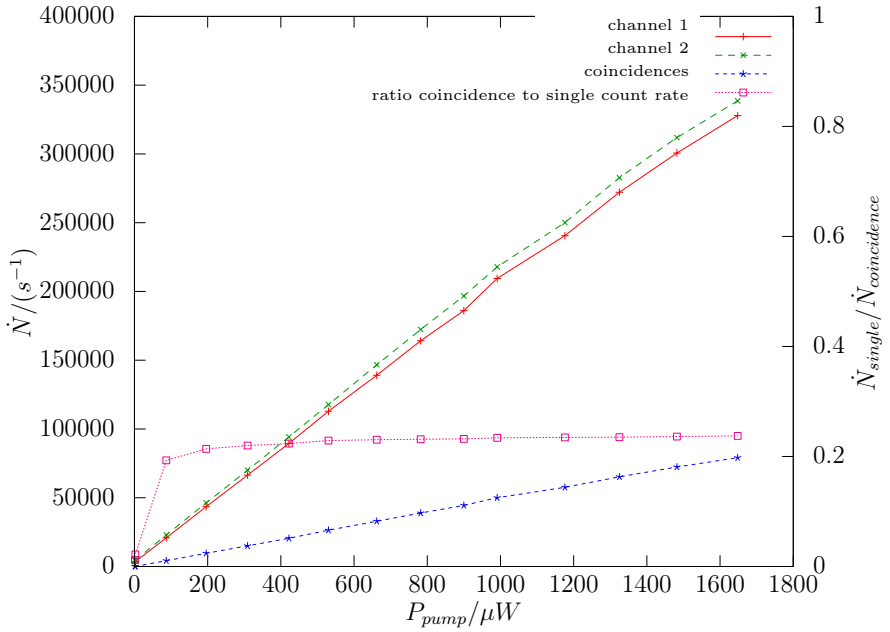

Figure 4.1.: Efficiency of SPDC. The ratio of coincidence and single count rates remains constant over a wide range of the laser power pumping the down-conversion crystal.

4.2. Interferometers

The interferometers are constructed by making use of a combination of fiber paths, fused fiber couplers (FFC) and free space delays (see Figure 4.2). This configuration exploits advantages of both concepts.

One of them is that the path lengths in the fibers vary on a larger time scale compared to free space paths. Therefore the fused fiber couplers require mere passive temperature stabilization. At the same time they offer a good mode overlap which leads to a good interference visibility as required for observing a high entanglement quality. The splitting ratio of $(50 \pm 2)\,\%$ is comparable to bulk beam splitters. Similarly the dimensionality of the states created can be doubled by just adding another pair of interferometers twice the length of the preceding interferometers. A detrimental effect of the fibers arises in this experiment as they are employed for near infrared wavelengths and not for telecom wavelengths. For the latter there are commonly used techniques to compensate chromatic dispersion.

The delays, i. e. the long interferometer arms, are implemented as free space paths. These offer a lower chromatic dispersion compared to fibers. By equalizing the fiber path lengths in the short and the respective long interferometer

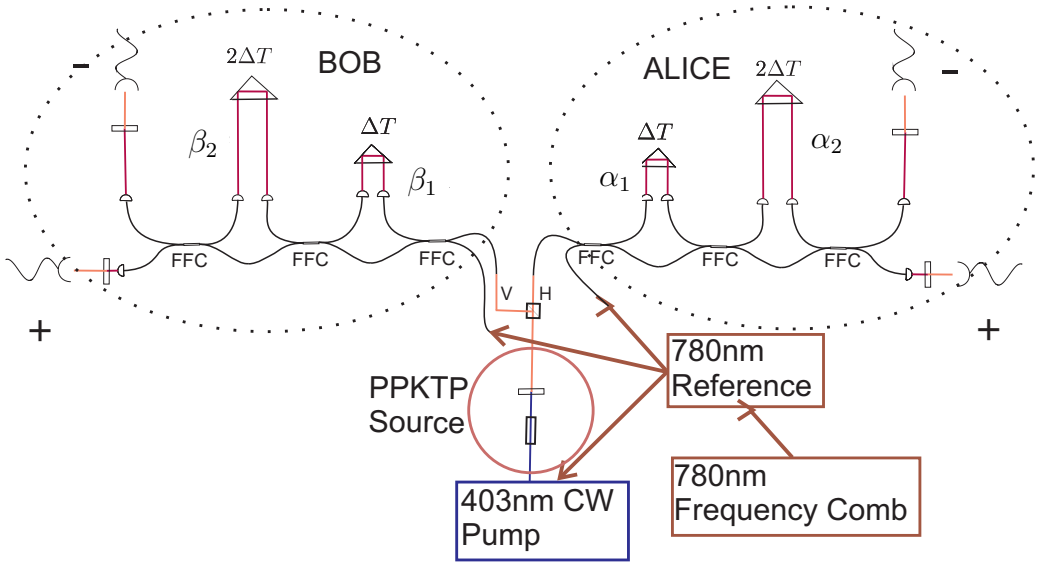

Figure 4.2.: Experimental setup. The interferometer systems are constructed of fibers (black), fused fiber couplers (FFC) and free space delays (red). Each party, Alice as well as Bob, is provided with two single photon detectors labeled "+" and "-". All interferometers as well as the laser pumping the periodically poled $KTiOPO_4$ crystal (PPKTP) are stabilized through the same reference laser which itself is referenced to a frequency comb mode.

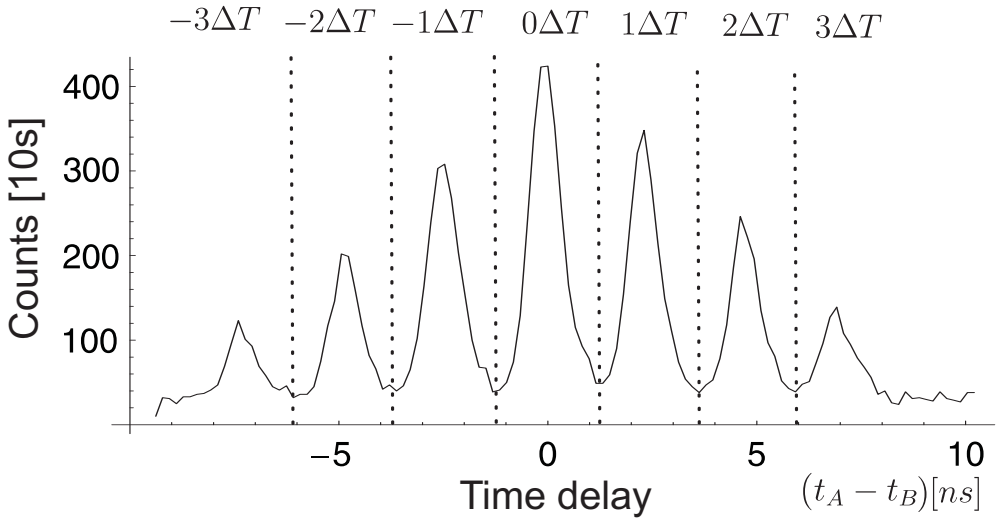

Figure 4.3.: Coincidence histogram. t_A and t_B denote the detection times of Alice's and Bob's photon, respectively. The time delay unit ΔT is chosen long enough to let the count rate minima separating the coincidence windows $-3\Delta T, \ldots, 3\Delta T$ approach the level of the background counts.

arm the overall chromatic dispersion can be kept small. The total delay acquired in the long arms of the first interferometers is $\Delta T = (2.4 \pm 0.1)$ ns.

4.3. Detection

The detection of the down-conversion photons at the outputs of the interferometers is accomplished by single photon avalanche photo diodes (APD).[2] As the minimal time delay ΔT depends on the detection timing resolution it would be advantageous to use commercial shallow junction APDs with resolutions down to ≈ 50 ps but reach-through APDs were chosen because they still offer a better detection efficiency. The typical timing resolution of 300 to 500 ps of the used APDs results in the constraint

$$\Delta T \geq (2.4 \pm 0.1)\,\text{ns}$$

imposed by the effective photon pair timing resolution for a critical level approaching the background counts (see Figure 4.3).

[2] quadruple single photon counting module model SPCM-AQ4C manufactured by PerkinElmer; involves four independent thick APDs

A time-to-digital converter[3] measures the delay between the photons of a coincident pair. The timing resolution of 80 ps of this computer controlled module is better than the APDs' resolution.

4.4. Stabilization

In order to observe the desired interference effects the experimental setup has to be adjusted and stabilized accordingly. The delays implemented by the four interferometers have to be equalized with respect to each other within the coherence length of the down-conversion photons. Moreover, a stable, well-defined phase relation between the superposing basis states is required at least for measurement times of about 1/2 h. Consequently the difference in length between short and long arm of an interferometer must be stabilized with subwavelength accuracy.

This requirement is counteracted mainly by temperature drifts in the surrounding air and components on a larger time scale and by vibrations of the optical table on a shorter time scale. The variation $\Delta\gamma$ of the relative phase γ between the spatial modes corresponding to an interferometer's short and long arm, respectively, is influenced by variations of the delay's length as well as by fluctuations of the pumping laser's wavelength. So not only the interferometers themselves must be stabilized but also the frequency of the pumping laser.

Thus, a maser referenced frequency comb mode with 250 kHz FWHM at 780 nm central wavelength is used to lock a reference laser. The latter is a grating stabilized diode laser operated at the same wavelength of 780 nm. Beside the stabilization of the interferometers through piezoactuator driven translation stages the reference laser is used to stabilize the pump laser frequency through a transfer cavity which is referenced by the Hänsch-Couillaud method [18]. The same procedure is used to stabilize the cavity to the reference laser.

The reference laser at 780 nm and the SPDC photons at 806 nm travel the same paths through the interferometers. Thus they can be chromatically separated. In addition, a polarization multiplexing scheme more detailed described in [30] is applied. Finally time multiplexing of the stabilization laser signal allows for independent stabilization of all interferometers.

In the following sections typical measurements on the coincidence count rates in dependence of the phases in the four interferometers are presented. The measurements are compared to the theoretical predictions from Section 2.7.

[3] model TDC-GPX manufactured by ACAM

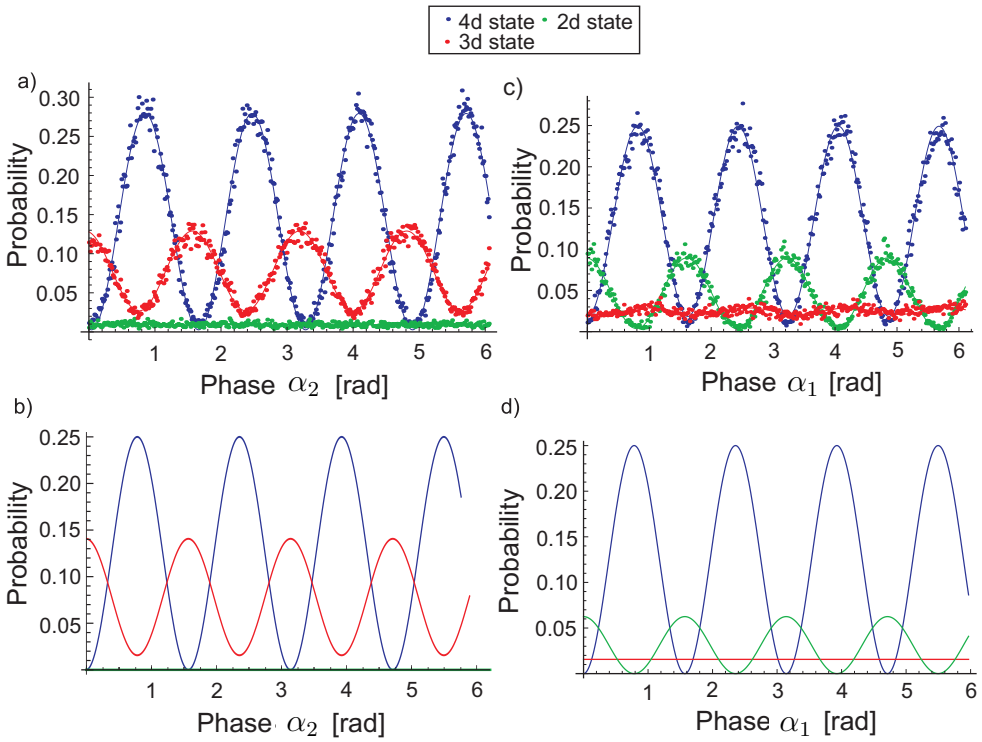

Figure 4.4.: Coincidence count rates in the $+,+$ detector combination and theoretical predictions as functions of phase α_2 (a,b) and phase α_1 (c,d) for the coincidence windows $0\Delta T, 1\Delta T$ and $2\Delta T$.

4.5. Scans of single interferometers

Here coincidence count rates observed for relative detection delays $\pm 2\Delta T, \pm 1\Delta T$ and $0\Delta T$ are presented as functions of one of the phases in the interferometers while the respective other phases were kept at a constant value. At the end of this section it will be explained in brief how the method of scanning was also applied in order to adjust and calibrate the setup.

Figure 4.4a shows the coincidence count rates recorded in the $+,+$ detector combination during a scan of Alice's second interferometer. In order to enable the comparison with the theoretical predictions, the corresponding coincidence functions from Table 2.3 on page 19 are plotted in Figure 4.4b. As α_1 and β_1 both are zero the coincidence probability

$$p(0\Delta T, +, +) = \frac{1}{4}\cos^2\left(\frac{\alpha_1 + \beta_1}{2}\right)\cos^2\left(\frac{\alpha_2 + \beta_2}{2}\right)$$

varies with the maximal fringe visibility of 1. The corresponding fit of the measured count rates allows to extract a fringe visibility of $V_{0\Delta T,\alpha_2} = 0.964 \pm 0.010$.

Table 4.1.: Measured interference visibilities of coincidence curves and corresponding theoretical expectations.

	experiment	theory	$\frac{\text{experiment}}{\text{theory}}$
$V_{0\Delta T,\alpha_2}$	0.964 ± 0.010	1	0.964 ± 0.010
$V_{1\Delta T,\alpha_2}$	0.664 ± 0.010	$7/9 = 0.\bar{7}$	0.854 ± 0.013
$V_{2\Delta T,\alpha_2}$	0	0	—
$V_{2\Delta T,\alpha_1}$	0.896 ± 0.010	1	0.896 ± 0.010

Table 4.1 on page 43 comprehensively lists the visibilities calculated from the experimental data together with the corresponding theoretical expectations. For the $1\Delta T$ coincidences the theoretical coincidence function has a visibility of $7/9 = 0.\bar{7}$. For the measured data a fringe visibility of $V_{1\Delta T,\alpha_2} = 0.664 \pm 0.010$ was calculated. The fringe visibility for the $2\Delta T$ coincidence count rate vanishes in clear correspondence with the theoretical prediction. A phase offset between the $0\Delta T$ and $1\Delta T$ coincidence curves of $\Delta\phi_{0\Delta T,1\Delta T} = (1.024 \pm 0.002)\pi$ was calculated for the cosine functions fitted to the experimental data. The theoretical expectation is π.

When plotted as a function of α_1 the theoretical coincidence probability

$$p\left(-1\Delta T,+,+\right) = \frac{1}{64}\left(3 - 2\cos\left(\left(\alpha_1 - \beta_1\right) - \alpha_2\right) - 2\cos\left(\alpha_2 + \beta_2\right) + 2\cos\left(\left(\alpha_1 - \beta_1\right) + \beta_2\right)\right) \tag{4.1}$$

stays at a constant level of $1/64$ if $\alpha_2 = -\beta_2$ in comparison to the achievable maximum of $9/64$ (see Figure 4.4d). The corresponding scan of the $1\Delta T$ coincidence count rate shows the same behaviour as the phases in the second interferometers fulfill $\alpha_2 = -\beta_2 = 0$. The visibility of the $2\Delta T$ coincidence count rate scan amounts to $V_{2\Delta T,\alpha_1} = 0.896 \pm 0.010$ which closely corresponds to the theoretical expectation of $V_{2\Delta T} = 1$. This scan yields a phase offset for α_1 of $\Delta\phi_{0\Delta T,2\Delta T} = (1.013 \pm 0.002)\pi$ between the interference curves of the $0\Delta T$ and $2\Delta T$ coincidences in comparison to the theoretical prediction of π.

As the probability for distributing the coincidences within any of the 7 coincidence windows is different, the signal to noise-ratio is different, too. The contribution of accidental coincidences can be estimated by triggering on coincedences with time delay difference $\Delta t_{\text{pair}} \gg 3\Delta T$ where no coincidence events caused by SPDC photon pairs are expected. This contribution amounts to about 1% of the maximal count rate observed in the $(0\Delta T,+,+)$ coincidence window. In contrast, this background count rate corresponds to about 4% of

the maximal count rates of the $2\Delta T$ states, limiting their fringe visibilities.

The interference curve patterns specific to the interferometer system were used to calibrate the different adjustable phases. The procedure is briefly explained in the following. A minimum of the $\pm 2\Delta T$ coincidence count rates is obtained by adjusting the phases in the first interferometers to

$$\alpha_1 + \beta_1 = 0 \tag{4.2}$$

(see Table 2.3 on page 19). In order to satisfy this equation α_1 and β_1 are always varied by the same absolute value but with opposite signs for the subsequent steps. By adjusting α_1 and β_1 such that the count rate of the $1\Delta T$ coincidences in the "+, +" detector combination is constant during the scan of the phase α_2 the equation

$$\alpha_1 = \beta_1 - \beta_2 \tag{4.3}$$

has to be fulfilled. Finally the phase α_2 is adjusted such that the count rate of the $0\Delta T$ coincidences in the "+, +" detector combination is maximal giving

$$\alpha_2 + \beta_2 = 0. \tag{4.4}$$

The phase β_2 remains as a free parameter which can be defined as

$$\beta_2 := 0. \tag{4.5}$$

Together (4.2), (4.3), (4.4) and (4.5) yield

$$\alpha_1 = \beta_1 = \alpha_2 = \beta_2 = 0.$$

Furthermore the fringe visibilities serve as a measure for the equality of the time delays in the different interferometers. In addition to the advantages mentioned already in Section 4.2 the free space implementation of the delays in the long interferometer arms facilitates blocking and thereby enables to select which paths should interfere.

By blocking the long arms of both second interferometers and varying the phase α_1 or β_1 interference is only possible for the two-party states $|0,0\rangle$ and $|1,1\rangle$. Maximizing the fringe visibility of the $0\Delta T$ coincidences by adjusting the length of the free space path in Alice's or Bob's first interferometer allows to maximize the overlap of the two-party states $|0,0\rangle$ and $|1,1\rangle$ as well. Hence the time delays $\Delta T_{a_1}, \Delta T_{b_1}$ implemented in Alice's and respecitvely Bob's first interferometer satisfy

$$\Delta T_{b_1} = \Delta T_{a_1} \tag{4.6}$$

up to the coherence time $t_{c,\mathrm{SPDC}}$ of the SPDC photons which obey $t_{c,\mathrm{SPDC}} \overset{(2.7)}{\ll} \Delta T_{a_1}$.

Similarly by blocking only Bob's second interferometer and scanning one of the phases α_1, β_1 or α_2 interference of the basis states $|2,1\rangle$ and $|1,0\rangle$ is observed in the $1\Delta T$ coincidence window. When the fringe visibility has been maximized by adjusting the length of the free space path in Alice's second interferometer the corresponding delay ΔT_{a_2} satisfies

$$\Delta T_{a_2} - \Delta T_{b_1} = \Delta T_{a_1} \overset{(4.6)}{\Longrightarrow} \Delta T_{a_2} = 2\Delta T_{a_1}. \tag{4.7}$$

Analogously to the equalization of the short interferometers the delay ΔT_{b_2} in Bob's long interferometer can be adjusted by blocking both first interferometers, yielding

$$\Delta T_{b_2} = \Delta T_{a_2} \overset{(4.7)}{=} 2\Delta T_{a_1}.$$

4.6. Influence of higher-dimensional states

Simultaneous scan of a short and a long interferometer

A simultaneous scan of the phase in a short and a long interferometer illustrates the difference between the four-dimensional entangled state registered by triggering on coincidences with no relative time delay and a two-dimensional state. In Figure 4.5 the phases α_1 and β_2 were scanned synchronously while the other phases were kept constant at $\alpha_2 = \beta_1 = 0$. The resulting dependence of the $0\Delta T$ coincidence count rate on the sum $\alpha_1 + \beta_2$ is $\propto \cos^4(\alpha_1 + \beta_2)$ whereas the theoretical expectation for the coincidence count rate corresponding to a two-dimensional state would be proportional to $\cos^2(\alpha_1 + \beta_2)$. The latter is plotted in the figure as well.

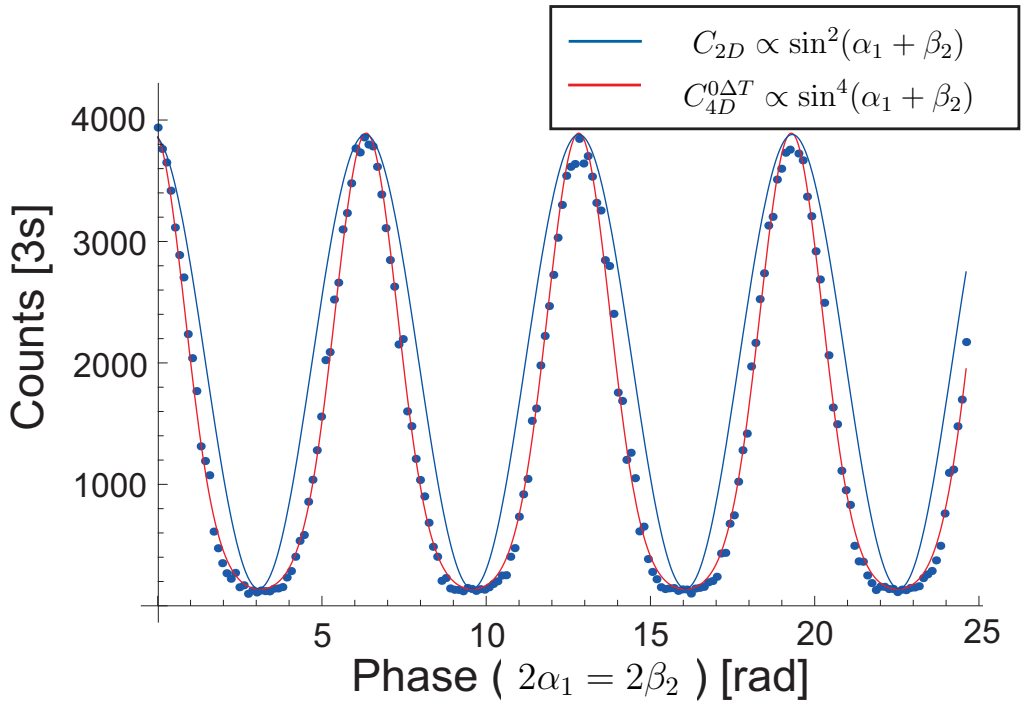

Figure 4.5.: Synchronous scan of the phases α_1 and β_2. The other phases are kept constant at $\alpha_2 = \beta_1 = 0$. The resulting dependence of the $0\Delta T$ coincidence count rate on the sum $\alpha_1 + \beta_2$ is $\propto \cos^4(\alpha_1 + \beta_2)$ as it corresponds to a four-dimensional state. This function is fitted to the experimental data. For comparison the theoretical coincidence function $\propto \cos^2(\alpha_1 + \beta_2)$ of a two-dimensional state is plotted there as well.

5. Bell tests

5.1. Considering coincidence windows separately

$0\Delta T$-Coincidences

Two different Bell inequalities were tested triggering on coincidences with relative time delay $0\Delta T$, the CHSH inequality and a CGLMP inequality.

CGLMP inequality

Tests of a CGLMP inequality described in Section 3.3 are presented which were performed by resorting to the choice of the basis described in Section 3.3.

The tested expression derived from (3.21) for $d = 4$ is

$$\begin{aligned} I_4 = & \\ & \Big\{ \big[Q(A_1 = B_1) \quad + Q(B_1 = A_2 + 1) + Q(A_2 = B_2) \quad + Q(B_2 = A_1)\big] \\ & -\big[Q(A_1 = B_1 - 1) + Q(B_1 = A_2) \quad + Q(A_2 = B_2 - 1) + Q(B_2 = A_1 - 1)\big]\Big\} \\ & +\frac{1}{3}\Big\{ \big[Q(A_1 = B_1 + 1) + Q(B_1 = A_2 + 2) + Q(A_2 = B_2 + 1) + Q(B_2 = A_1 + 1)\big] \\ & -\big[Q(A_1 = B_1 - 2) + Q(B_1 = A_2 - 1) + Q(A_2 = B_2 - 2) + Q(B_2 = A_1 - 2)\big]\Big\}. \end{aligned} \tag{5.1}$$

In this case each of the 16 expressions for Q is a sum of four coincidence probabilities according to (3.20). So the Bell test requires the measurement of relative coincidence frequencies for 64 combinations of the phases $\alpha_1, \alpha_2, \beta_1$ and β_2.

According to (3.23) these phases to be set in the respective interferometers are sums of the respective phases corresponding to the output projector for the single outcomes $0, 1, 2$ or 3 and of the numerically calculated preparation phases corresponding to the observable A_1, A_2, B_1 or B_2 respectively. The

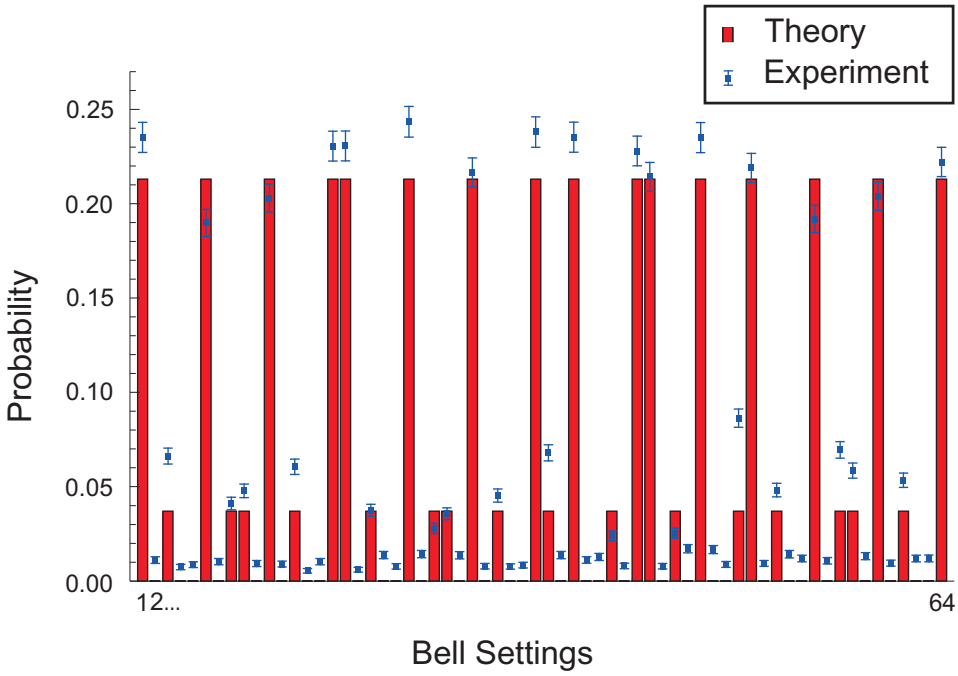

Figure 5.1.: Theoretical and measured probabilities of the $0\Delta T$ coincidences in the "+, +" detector pair for the 64 sets of phases $\{\alpha_1, \alpha_2, \beta_1, \beta_2\}$ for which the CGLMP expression I_4 reaches its maximal value (see (5.1)).

optimized phases yielding the maximal value

$$\max_{\text{QM}}(I_4) = \frac{2}{3}\left(1 + 2\sqrt{2}\right) \approx 2.552$$

theoretically achievable for this experiment are

$$\begin{array}{llll} \alpha_1''(A_1) = 0.431, & \alpha_2''(A_1) = -0.007, & \beta_1''(B_1) = -1.216, & \beta_2''(B_1) = 0.007, \\ \alpha_1''(A_2) = -1.140, & \alpha_2''(A_2) = -0.007, & \beta_1''(B_2) = 0.355, & \beta_2''(B_2) = 0.007\,. \end{array}$$

In Figure 5.1 the computed theoretical expectations for the coincidence probabilities as well as the corresponding measured probabilities are plotted for all 64 phase combinations.

The value of the expression calculated for the experimental data is

$$I_4 = 2.421 \pm 0.012$$

which surpasses the bound $\max_{\text{local variable}}(I_4) = 2$ by 35 standard deviations.

CHSH inequality

The following test of a CHSH inequality is a test of the experimental scheme for two-dimensional entangled states originally proposed by Franson [16] in 1989. This statement is true in the following sense.

As for each SPDC photon of a pair there is only a single path leading from the source to the respective interferometer system no interference of spatial two-photon modes can occur. Consequently the splitting ratio between the event "Bob's photon takes the same beam splitter output as Alice's photon" and the event "Bob's photon takes output $\mp$ if Alice's photon takes output $\pm$" is completely random i. e. the probabilities for both events are $1/2$. If Alice's and Bob's photon share the output mode after the first beam splitter they can only acquire a time delay of $0\Delta T$ or $\pm 2\Delta T$ such that

$$p_{\pm 2\Delta T} + p_{0\Delta T,x} + p_{0\Delta T,y} = 1/2 \tag{5.2}$$

holds (see Table 2.4 on page 20 for definitions of the summed probabilities). For the other events

$$p_{\pm 3\Delta T} + \sum_{i=x,y,w,z} p_{\pm 1\Delta T,i} = 1/2 \tag{5.3}$$

is fulfilled. By postselection of the $0\Delta T$ coincidences all events that contribute to (5.3) are dropped. As $\alpha_1 = \beta_1 = 0$ for all measurement settings in this test (see (5.5)), $p_{\pm 2\Delta T} = 0$ holds and in principle all coincidences that contribute to (5.2) are registered in the $0\Delta T$ time delay window. In the original Franson experiment half of all coincidences are postselected in the $0\Delta T$ time delay window as well. So the correlation function used here is the same as for the test of the CHSH inequality in the original Franson setup:

$$C_{\mathrm{CHSH},0\Delta T} = \frac{p_{0\Delta T,x} - p_{0\Delta T,y}}{p_{0\Delta T,x} + p_{0\Delta T,y}} = \frac{[p\,(0\Delta T,+,+) + p\,(0\Delta T,-,-)] - [p\,(0\Delta T,+,-) + p\,(0\Delta T,-,+)]}{[p\,(0\Delta T,+,+) + p\,(0\Delta T,-,-)] + [p\,(0\Delta T,+,-) + p\,(0\Delta T,-,+)]}$$

A set of phases allowing to maximally violate the CHSH inequality

$$-2 \leq I_{\mathrm{CHSH},0\Delta T} = C_{\mathrm{CHSH},0\Delta T}(A_1,B_1) + C_{\mathrm{CHSH},0\Delta T}(A_1,B_2) + C_{\mathrm{CHSH},0\Delta T}(A_2,B_1) - C_{\mathrm{CHSH},0\Delta T}(A_2,B_2) \leq 2, \tag{5.4}$$

by the value $\max_{\mathrm{QM}}(I_{\mathrm{CHSH},0\Delta T}) = 2\sqrt{2}$ consists of

$$\begin{aligned} &\alpha_1(A_1) = 0, && \alpha_2(A_1) = -\frac{\pi}{4}, && \beta_1(B_1) = 0, && \beta_2(B_1) = 0, \\ &\alpha_1(A_2) = 0, && \alpha_2(A_2) = \frac{\pi}{4}, && \beta_1(B_2) = 0, && \beta_2(B_2) = \frac{\pi}{2}. \end{aligned} \tag{5.5}$$

The experimental value for the CHSH expression extracted from the measured data is

$$I_{\mathrm{CHSH},0\Delta T} = 2.51 \pm 0.04$$

which surpasses the bound $\max_{\text{local variable}}(I_{\mathrm{CHSH},0\Delta T}) = 2$ for local variable models by 12.8 standard deviations.

$\pm 1\Delta T$-Coincidences

On the coincidences postselected within the time delay window $\pm 1\Delta T$ the CGLMP expression I_3 was tested (see (3.22)). It resembles the expression I_2 except for the form of the sums $Q(A_a = B_b + n)$, $a, b \in \{1, 2\}$, $n \in \mathbb{N}$ (see (3.20)). In the expression I_2 each of the sums consists of two coincidence probabilities $P\left(A_a = i, B_b = (i + n) \bmod d\right)$ whereas in I_3 tested here each Q consists of three coincidence probabilities, resulting in a total of 24 coincidence probabilities to be measured.

In order to enable the distinction of different outcomes at each party a change of basis as described in Section 3.3 was applied. In this case only three different single outcomes are required and the corresponding new basis states described in terms of the old basis are

$$\begin{aligned}
|\phi_0\rangle &:= \frac{1}{\sqrt{3}}\big(\,|0\rangle \qquad + |1\rangle \qquad + |2\rangle\big),\\
|\phi_1\rangle &:= \frac{1}{\sqrt{3}}\big(\,|0\rangle + \mathrm{e}^{\mathrm{i}1\cdot 2\pi/3}\,|1\rangle + \mathrm{e}^{\mathrm{i}2\cdot 2\pi/3}\,|2\rangle\big),\\
|\phi_2\rangle &:= \frac{1}{\sqrt{3}}\big(\,|0\rangle + \mathrm{e}^{\mathrm{i}2\cdot 2\pi/3}\,|1\rangle + \mathrm{e}^{\mathrm{i}1\cdot 2\pi/3}\,|2\rangle\big),
\end{aligned}$$

for one party and

$$\begin{aligned}
|\varphi_0\rangle &:= \frac{1}{\sqrt{3}}\big(\,|1\rangle \qquad + |2\rangle \qquad + |3\rangle\big),\\
|\varphi_1\rangle &:= \frac{1}{\sqrt{3}}\big(\,|1\rangle + \mathrm{e}^{\mathrm{i}2\cdot 2\pi/3}\,|2\rangle + \mathrm{e}^{\mathrm{i}1\cdot 2\pi/3}\,|3\rangle\big),\\
|\varphi_2\rangle &:= \frac{1}{\sqrt{3}}\big(\,|1\rangle + \mathrm{e}^{\mathrm{i}1\cdot 2\pi/3}\,|2\rangle + \mathrm{e}^{\mathrm{i}2\cdot 2\pi/3}\,|3\rangle\big),
\end{aligned}$$

for the other party. They can be implemented for the "+" detectors by accordingly adjusting the phases in the interferometers such that

$$|\phi\rangle = \frac{1}{\sqrt{3}}(|0\rangle + \mathrm{e}^{\mathrm{i}\gamma_1'}\,|1\rangle + \mathrm{e}^{\mathrm{i}\gamma_2'}\,|2\rangle)$$

and respectively

$$\begin{aligned} |\varphi\rangle &= \frac{1}{\sqrt{3}}(\mathrm{e}^{\mathrm{i}\gamma_1''}|1\rangle + \mathrm{e}^{\mathrm{i}\gamma_2''}|2\rangle + \mathrm{e}^{\mathrm{i}(\gamma_1''+\gamma_2'')}|3\rangle) \\ &= \mathrm{e}^{\mathrm{i}\gamma_1''}\frac{1}{\sqrt{3}}(|1\rangle + \mathrm{e}^{\mathrm{i}(\gamma_2''-\gamma_1'')}|2\rangle + \mathrm{e}^{\mathrm{i}\gamma_2''}|3\rangle) \end{aligned}$$

hold where the global phase can be dropped. Here phase shifts introduced by the beam splitters contribute to the phases $\gamma_1', \gamma_2', \gamma_1''$ and γ_2''.

The quantum mechanical maximum for I_3 of $\max_{\mathrm{QM}}(I_3) = \frac{4}{3}\cdot(1+\sqrt{\frac{4}{3}}) \approx 2.87$ is reached for

$$\begin{aligned} &\alpha_1''(A_1) = -\frac{\pi}{3}, \quad &&\alpha_2''(A_1) = -\frac{\pi}{6}, \quad &&\beta_1''(B_1) = -\frac{\pi}{2}, \quad &&\beta_2''(B_1) = \pi, \\ &\alpha_1''(A_2) = 0, \quad &&\alpha_2''(A_2) = -\frac{\pi}{2}, \quad &&\beta_1''(B_2) = \frac{\pi}{6}, \quad &&\beta_2''(B_2) = 0. \end{aligned}$$

The theoretical expectations for all 24 probabilities $P\big(A_a = i, B_b = (i+n) \bmod d\big)$ appearing in the expression I_3 are plotted in Figure 5.2 together with the measured relative frequencies of the corresponding coincidence events.

From the experimental data a value for the CGLMP expression of $I_3 = 2.68 \pm 0.05$ was calculated. This result represents a violation of the bound $\max_{\text{local variable}}(I_3) = 2$ by 13.6 standard deviations, therefore proving intrinsic three-dimensional entanglement.

$\pm 2\Delta T$-Coincidences

Concerning the $\pm 2\Delta T$ coincidences there is no information which can be extracted by defining a correlation function between the probabilities of detection at different output modes. This is so as the coincidence probability is the same for all output combinations, i. e. for $(+,+), (+,-), (-,+)$ and $(-,-)$. Thus, for a postselection of the $+\Delta 2$ or $-\Delta 2$ coincidences the correlation function is defined by resorting to a change of basis as described in 3.3.

The states forming the new basis of the postselected subspace read

$$\begin{aligned} |\theta_0\rangle &:= \frac{1}{\sqrt{2}}\big(|0\rangle + |1\rangle\big), \\ |\theta_1\rangle &:= \frac{1}{\sqrt{2}}\big(|0\rangle - |1\rangle\big), \end{aligned}$$

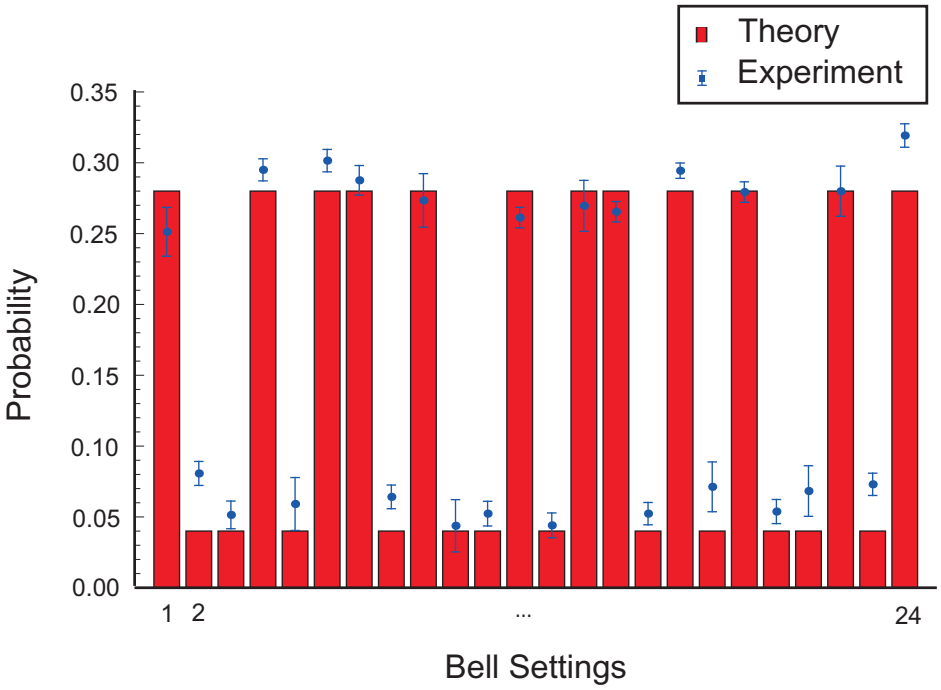

Figure 5.2.: Theoretical and measured coincidence probabilities of the $\pm 1 \Delta T$ coincidences in the "+, +" detector pair for the 24 sets of phases $\{\alpha_1, \alpha_2, \beta_1, \beta_2\}$ for which the CGLMP expression I_3 (see (3.22)) is maximized.

for one party and

$$|\vartheta_0\rangle := \frac{1}{\sqrt{2}}\big(\,|2\rangle + |3\rangle\big),$$
$$|\vartheta_1\rangle := \frac{1}{\sqrt{2}}\big(\,|2\rangle - |3\rangle\big),$$

for the other party. They can be implemented by accordingly adjusting the phases α_1 and β_1. The preparation phases which maximize the absolute value of the CHSH expression are

$$\alpha_1''(A_1) = -\frac{\pi}{4}, \qquad \alpha_2''(A_1) = 0, \qquad \beta_1''(B_1) = 0, \qquad \beta_2''(B_1) = 0,$$
$$\alpha_1''(A_2) = \frac{\pi}{4}, \qquad \alpha_2''(A_2) = 0, \qquad \beta_1''(B_2) = \frac{\pi}{2}, \qquad \beta_2''(B_2) = 0,$$

and give the theoretically maximal quantum value of

$$\max_{\mathrm{QM}} |I_{\mathrm{CHSH}}| = 2\sqrt{2} \approx 2.828\,.$$

The corresponding measured correlations are

$$\begin{aligned} C_{\mathrm{CHSH}}(A_1, B_1) &= -0.619 \pm 0.004, \\ C_{\mathrm{CHSH}}(A_1, B_2) &= -0.653 \pm 0.004, \\ C_{\mathrm{CHSH}}(A_2, B_1) &= -0.714 \pm 0.004, \\ C_{\mathrm{CHSH}}(A_2, B_2) &= 0.487 \pm 0.004\,. \end{aligned}$$

The associated CHSH expression amounts to

$$|I_{\mathrm{CHSH}}| = 2.475 \pm 0.007$$

which means a violation of the bound $\max_{\text{local variable}} |I_{\mathrm{CHSH}}| = 2$ for local variable theories by 68 standard deviations for an integration time of 10 seconds.

5.2. Including time delay detection basis

As it was explained in Section 2.7, for specific subsets of all distinguishable coincidence events, correlation functions can be defined such that the sum of the contributing coincidence events remains constant.

The subset of coincidence events that this method was applied to consists of all coincidence events with relative time delay $0\Delta T$ and $\pm 2\Delta T$ whose probabilities add up to the constant value of $1/2$ (see (2.14)). Measurements on the corresponding correlation functions C_1 and C_2 defined in (2.15) and (2.16) are presented.

CHSH

The correlation function

$$C_1 = \frac{(p_{0\Delta T,x} + p_{0\Delta T,y}) - p_{\pm 2\Delta T}}{(p_{0\Delta T,x} + p_{0\Delta T,y}) + p_{\pm 2\Delta T}} = \cos(\alpha_1 + \beta_1)$$

resembles the correlation function used in the original Franson experiment for a test of the CHSH inequality. This can be understood in the following manner.

Compare the setup of the original Franson experiment and the setup used here (see Figure 2.1 and Figure 2.2). The "+, −" coincidence event with no relative time delay in the Franson setup is mapped to a $-2\Delta T$ coincidence in the setup used in this experiment. The $0\Delta T$ "−, +" coincidence event in the Franson setup corresponds to a $+2\Delta T$ coincidence in the setup used here. And the $0\Delta T$ "+, +" and "−, −" coincidences in the Franson case are mapped to $0\Delta T$ coincidences detected at any output combination in this experiment.

Thus a CHSH inequality consisting of correlations $C_1(A_a, B_b)$ of observables A_a, B_b, $a, b \in \{1, 2\}$ at Alice's and respectively Bob's side was tested:

$$-2 \leq C_1(A_1, B_1) + C_1(A_1, B_2) + C_1(A_2, B_1) - C_1(A_2, B_2) \leq 2 \qquad (5.6)$$

The phases which theoretically allow to reach the maximum of $\max_{\mathrm{QM}}(I_{\mathrm{CHSH}}) = 2\sqrt{2} \approx 2.83$ are

$$\begin{aligned} &\alpha_1(A_1) = 0, && \alpha_2(A_1) = 0, && \beta_1(B_1) = -\frac{\pi}{4}, && \beta_2(B_1) = 0, \\ &\alpha_1(A_2) = \frac{\pi}{2}, && \alpha_2(A_2) = 0, && \beta_1(B_2) = \frac{\pi}{4}, && \beta_2(B_2) = 0. \end{aligned} \qquad (5.7)$$

For the CHSH expression a value of

$$2.29 \pm 0.04$$

was calculated from the experimental data. This result violates the upper bound $\max_{\text{local variable}}(I_{\mathrm{CHSH}}) = 2$ by 7 standard deviations.

Bell tests for the correlation function C_2

The expression tested for the correlation function C_2 is similar to the CHSH expression except for the different definition of the correlations:

$$I_{C_2} := C_2(A_1, B_1) + C_2(A_1, B_2) + C_2(A_2, B_1) - C_2(A_2, B_2),$$

$$\begin{aligned} C_2 &:= \frac{p_{0\Delta T,x} - p_{0\Delta T,y} - p_{\pm 2\Delta T}}{p_{0\Delta T,x} + p_{0\Delta T,y} + p_{\pm 2\Delta T}} \\ &= \cos^2\left(\frac{\alpha_1 + \beta_1}{2}\right)\cos(\alpha_2 + \beta_2) - \sin^2\left(\frac{\alpha_1 + \beta_1}{2}\right) \end{aligned}$$

The bounds of this expression for correlations that can be described by a local variable model were computed resorting to the method explained in Section 3.2:

$$\begin{aligned} \min_{\text{local variable}}(I_{C_2}) &= -4, \\ \max_{\text{local variable}}(I_{C_2}) &= 2. \end{aligned}$$

The theoretical minimum of the correlations yielded for the setup described in this work is the same as for local variable models: $\min_{\text{QM}}(I_{C_2}) = -4$. A set of phases allowing to surpass the bound $\max_{\text{local variable}}(I_{C_2}) = 2$ by a maximum of $\max_{\text{QM}}(I_{C_2}) = 2\sqrt{2} \approx 2.83$ is

$$\begin{aligned} &\alpha_1(A_1) = 0, \quad &&\alpha_2(A_1) = -\frac{\pi}{4}, \quad &&\beta_1(B_1) = 0, \quad &&\beta_2(B_1) = 0, \\ &\alpha_1(A_2) = 0, \quad &&\alpha_2(A_2) = \frac{\pi}{4}, \quad &&\beta_1(B_2) = 0, \quad &&\beta_2(B_2) = \frac{\pi}{2}. \end{aligned} \tag{5.8}$$

From the measured data a value of

$$I_{C_2,(5.8)} = 2.59 \pm 0.04$$

was calculated. This represents a violation of the upper bound $\max_{\text{local variable}}(I_{C_2}) = 2$ for local variable models by 14.8 standard deviations.

An interesting detail about this Bell test is the fact that I_{C_2} yields a violation of the upper bound for the set of phases listed here in (5.8) where α_1 and β_1 constantly are zero as well as for the phases listed in (5.7) from the preceding test of the CHSH inequality where only the phases α_1 and β_1 were varied. Furthermore the set of phases listed in (5.8) is equivalent to the set of phases listed in (5.5) in Section 5.1. There a test of the CHSH inequality concerned with the pair of both second interferometers is described.

A test of the expression I_{C_2} with the set of angles listed in (5.7) yields a value of

$$I_{C_2,(5.7)} = 2.18 \pm 0.04$$

which lies above $\max_{\text{local variable}}(I_{C_2}) = 2$ by 4.5 standard deviations.

6. Discussion and future prospects

One of the main goals of this work was the characterization of the entanglement of experimentally prepared states through the measurement of two-photon interference and the test of suitable Bell type inequalities.

In Chapter 2 the framework of quantum mechanics was introduced necessary for the description of the experiment. Based on this, coincidence functions corresponding to different two-photon states were derived for the experimental setup which represents a higher-dimensional extension of the Franson experiment [16]. In the considered modification another pair of unbalanced interferometers allows for additional superpositions of interfering two-photon basis states. The coincidence events corresponding to these superpositions can be distinguished by the different relative time delays between the detections of the photons of a pair. In Section 4.5 the derived coincidence functions were consequently compared to measured coincidence curves (see Table 4.1 on page 43).

The ratios of the experimentally observed to the theoretically expected interference visibilities range from 0.854 ± 0.013 for coincidences with a relative time delay of $1\Delta T = (2.4 \pm 0.1)$ ns to 0.964 ± 0.010 for coincidences with no relative time delay. As it was mentioned in Section 4.5 these reduced visibilities can at least partially be ascribed to the different contributions of accidental coincidences to the count rates of the different coincidence events. Therefore, further reduction of background counts would be desirable.

The dimensionality of the Hilbert space corresponding to the coincidences with no relative time delay was demonstrated by a simultaneous scan of two different interferometers leading to a $\cos^4$ dependence. Also, the experimentally achieved visibilities as well as the observed phase offsets $\Delta\phi_{0\Delta T,1\Delta T} = (1.024 \pm 0.002)\pi$ and $\Delta\phi_{0\Delta T,2\Delta T} = (1.013 \pm 0.002)\pi$ with only small deviations from the expected value of π (see Section 4.5) demonstrate that the behaviour of the chosen experimental setup is close to the theoretical model.

In Chapter 5 several Bell inequalities were tested. Coincedence events with different relative time delays were considered separately as well as in suitable combinations. The results of all Bell tests violated the respective inequality's upper bound of 2 for local variable models by values ranging from $I_{C_2,(5.7)} =$

2.18 ± 0.04 over $I_{C_2,(5.8)} = 2.59 \pm 0.04$ to $I_3 = 2.68 \pm 0.05$.

In Section 2.7 the correlation function

$$\begin{aligned} C_2 &= \frac{p_{0\Delta T,x} - p_{0\Delta T,y} - p_{\pm 2\Delta T}}{p_{0\Delta T,x} + p_{0\Delta T,y} + p_{\pm 2\Delta T}} \\ &= \cos^2\left(\frac{\alpha_1 + \beta_1}{2}\right)\cos(\alpha_2 + \beta_2) - \sin^2\left(\frac{\alpha_1 + \beta_1}{2}\right) \end{aligned}$$

[1] was defined to preserve information about all correlations between the three classes of coincidence events it takes into account. Therefore the corresponding inequality I_{C_2} is violated for the two sets of phases that were optimized to give maximal violations of the CHSH inequality I_{CHSH} (see (5.6) on page 54) and I_{C_2} itself, respectively. In contrast, I_{CHSH} is not violated for the second set of phases as it is not defined to preserve information about all correlations between the classes of coincidence events taken into account.

Hence, I_{C_2} is non-redundant with respect to I_{CHSH} according to the definition given by Collins and Gisin [10]:

> "Given two inequalities which are violated, we define the first to be *non-redundant* if quantum mechanics gives a point $P(j_A, j_B|i_A, i_B)$ which violates the first inequality, but which does not violate the second inequality (or any inequality equivalent to the second)."[2]

In Section 3.3 a change of basis was introduced enabling the test of Bell inequalities for which a higher number of outputs where the photons can be detected would otherwise be necessary. It has to be checked if such changes of basis that were performed in order to test Bell inequalities on the coincidences postselected for relative time delay $0\Delta T$, $\pm 1\Delta T$ and $\pm 2\Delta T$ are feasible for applications in e. g. quantum key distribution (QKD). The applied method requires to *subsequently* measure the count rates of different coincidence events. Of course this is only necessary if all these count rates are needed for the specific chosen QKD scheme. Consequently, this procedure would require a longer measurement time and therefore could partially outweigh a higher data transfer rate owed to the higher dimensionality.

In the performed measurements that relied on a change of basis only the coincidence counts for a single output combination and relative time delay were taken into account. Therefore it could be investigated if changes of basis can be simultaneously implemented for different output combinations by the same set of phases $\alpha_1, \alpha_2, \beta_1, \beta_2$.

[1] $\alpha_1, \alpha_2, \beta_1, \beta_2$ denote the relative phases adjusted in the interferometers.
[2] $P(j_A, j_B|i_A, i_B)$ corresponds to a set of phases $\{\alpha_1, \alpha_2, \beta_1, \beta_2\}$.

In this thesis Bell inequalities for two observables, i. e. sets of phases, per party were tested. Other Bell inequalities [10], also for more than two observables [7], might be tested on the described experimental setup.

Furthermore the original Franson experiment is doubted to suit the needs for a test of local realism due to the postselection of 50 % of all events [1]. Theoretical investigations could answer the question whether the extension to higher dimensions represents a possibility to overcome this problem.

E. g. for the experimental setup that this thesis is concerned with, only $1/8$ of all coincidences, i. e. coincidences with a relative time delay of $3\Delta T$, cannot be influenced by the phases $\alpha_1, \alpha_2, \beta_1, \beta_2$ set in the interferometers.

So far, attempts that were undertaken during this work to define a correlation function which is suitable for the violation of a Bell inequality and which takes into account all coincidence events, or at least the ones that can be manipulated by the phases set in the interferometers, failed. A reason for this failure can be associated with the probabilistic splitting of all coincidence events into three classes (see (2.14) on page 18) leading to an upper bound of $1/2$ for every coincidence probability. In contrast, in an LHV model the probabilities p_a and p_b for some single events can reach the value one and hereby maximize the probability $p_a \cdot p_b = 1$ of the corresponding coincidence event. From a theoretical point of view, the contributions of the $\pm 1\Delta T$ coincidence windows add to a mixed state, limiting the violation of a suited Bell inequality.

During this work an additional stage of two similar interferometers was set up, each implementing a time delay of $4\Delta T$ for its long arm with respect to its short arm. The Hilbert space serving as a framework for the description of the system made up of three interferometer loops per party then is eight-dimensional. It will enable the test of further Bell inequalities for higher-dimensional systems possibly being exploitable for inherently secure quantum communication protocols.

A. Quasi-phasematching

The pairs of entangled photons used in the described experiment are produced by spontaneous parametric down-conversion (SPDC) [19]. In this process a pump photon of wavelength ω_p spontaneously decays into a pair of SPDC photons called signal and idler in a medium with a nonlinearity $\chi^{(2)}_{ijk}$ of second order in the polarisation's dependence on the electric field:

$$P^i = \epsilon_0(\chi^{(1)}_{ij}E^j + \chi^{(2)}_{ijk}E^jE^k + \cdots)$$

This nonlinearity also describes SPDC [27].

The wavelengths ω_s and ω_i of signal and respectively idler photon satisfy

$$\omega_p = \omega_s + \omega_i$$

as the photon energy is conserved in this process. Conservation of momentum completes the *quasi*-phasematching conditions:

$$\mathbf{k}_p\big(\lambda_p, n_p(\lambda_p, T)\big) = \mathbf{k}_s\big(\lambda_s, n_s(\lambda_s, T)\big) + \mathbf{k}_i\big(\lambda_i, n_i(\lambda_i, T)\big) + \frac{2\pi}{\Lambda(T)} \qquad \text{(A.1)}$$

Here $\mathbf{k}_j$ and $\lambda_j, j \in \{p, s, i\}$ are the wavevectors and wavelengths of pump, signal and idler photons respectively. The crystal's refractive indices $n_j, j \in \{p, s, i\}$ for the respective wave fields depend on their wavelengths and the temperature. The additional term, which accounts for the prefix "quasi-", depends on the crystal's poling period Λ as in the used periodically poled $KTiOPO_4$ (PPKTP) crystal the effective nonlinearity of the medium is periodically inverted. This property can be achieved by alternating an electric field during the fabrication of the crystal. Compared to phasematching in bulk nonlinear crystals, a broader range of phasematching angles and wavelengths is possible for quasi-phasematching in periodically poled crystals. Similarly it allows to warrant phasematching over directions of the crystal for which the effective nonlinearity and therefore the photon pair creation efficiency is increased. A significant advantage of the periodic poling is that the longitudinal and transversal walkoff between the SPDC photons is compensated allowing longer crystals.

The trajectories of signal and idler photon are constrained within two cones whose axes are symmetrically arranged with respect to the pump beam. The

SPDC process exploited in this experiment is of type-II [31]. I. e. not both SPDC photons are ordinarily polarized but one is extraordinarily polarized, while the pump photon is extraordinarily polarized with respect to the optical axis of the crystal. The chosen geometrical configuration is collinear, i. e. the emission cones of signal and idler photon contact in one line. Along this line signal and idler photon of a pair are indistinguishable in principle with respect to their spatial mode distribution. This fact gives rise to the desired entanglement.

The wavelengths of the SPDC photons should be degenerate at $\lambda_i = \lambda_s = 806\,\text{nm}$ for this experiment. According to the manufacturer of the crystal the ideal temperature allowing for this degeneracy is at $45.75\,^\circ\text{C}$ for a poling period of $9.675\,\mu\text{m}$. In the experiment the optimal temperature for the desired wavelength degeneracy turned out to be $(26.0 \pm 0.2)\,^\circ\text{C}$. For this value a poling period of $9.735\,\mu\text{m}$ can be computed in correspondence with calculations according to [14] (see also [21]). According to the manufacturer deviations in the range of $0.25\,\mu\text{m}$ can occur in the fabrication process. Moreover the Sellmeier coefficients incorporated in the calculations according to [14] are empirically determined for different wavelength regimes. Thus, the Sellmeier coefficients can lead to deviations for the wavelength regime from 400 to 800 nm covered here. Figure A.1 shows a plot of the measured wavelengths of the extraordinarily and ordinarily polarized SPDC photons in dependence of the crystal temperature. The theoretical curves calculated from (A.1) are plotted there as well for the grating periods of $9.675\,\mu\text{m}$ and $9.731\,\mu\text{m}$ respectively.

In order to maximize the efficiency of the SPDC process, i. e. the coincidence count rate, the pump beam focusing was adjusted to a waist of $w_p = 25\,\mu\text{m}$ in the crystal of length 10 mm according to measurements published by Fedrizzi et al. [15].

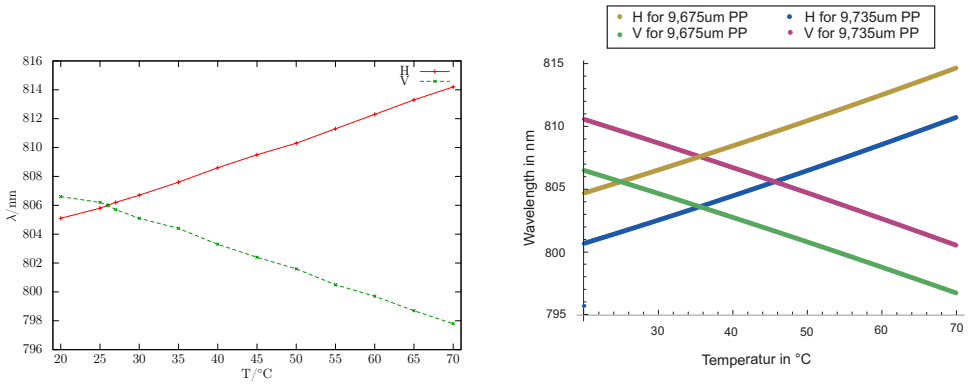

(a) (b)

Figure A.1.: Temperature dependence of down-conversion photon wavelengths as experimentally measured (A.1a) and theoretically predicted (A.1b). Signal and idler photon, together constituting a down-conversion pair, are orthogonally polarized with respect to each other.

Nomenclature

APD	avalanche photo diode
CGLMP	Collins, Gisin, Linden, Massar, and Popescu
CH	Clauser and Horne
EPR	Einstein, Podolsky, and Rosen
FFC	fused fiber coupler
FWHM	full width at half maximum
LHV	local hidden variable
PBS	polarizing beam splitter
PPKTP	periodically poled $KTiOPO_4$
SPDC	spontaneous parametric down-conversion

Bibliography

[1] Sven Aerts, Paul Kwiat, Jan-Åke Larsson, and Marek Zukowski. Two-photon franson-type experiments and local realism. *Phys. Rev. Lett.*, 83 (15):2872–2875, Oct 1999. doi: 10.1103/PhysRevLett.83.2872.

[2] Francois Arnault. A complete set of multidimensional bell inequalities. July 2011.

[3] J. S. Bell. On the einstein-podolsky-rosen paradox. *Physics*, 1:195, 1964.

[4] John S. Bell. On the problem of hidden variables in quantum mechanics. *Rev. Mod. Phys.*, 38:447–452, Jul 1966. doi: 10.1103/RevModPhys.38.447. URL `http://link.aps.org/doi/10.1103/RevModPhys.38.447`.

[5] John S. Bell. *John S. Bell on the foundations of quantum mechanics*. World Scientific, Singapore [u.a.], 2001. ISBN 981-02-4687-0 - 981-02-4688-9.

[6] John S. Bell. *Speakable and unspeakable in quantum mechanics*. Collected papers on quantum philosophy. Cambridge Univ. Press, Cambridge, 2. ed., revised ed. edition, 2004. ISBN 978-0-521-52338-7 - 0-521-81862-1. Bibliogr. J. Bell S. [VIII] - IX.

[7] Nicolas Brunner and Nicolas Gisin. Partial list of bipartite bell inequalities with four binary settings. *Physics Letters A*, 372(18):3162 – 3167, 2008. ISSN 0375-9601. doi: DOI:10.1016/j.physleta.2008.01.052. URL `http://www.sciencedirect.com/science/article/pii/S0375960108001710`.

[8] John F. Clauser and Michael A. Horne. Experimental consequences of objective local theories. *Phys. Rev. D*, 10(2):526–535, Jul 1974. doi: 10.1103/PhysRevD.10.526.

[9] John F. Clauser, Michael A. Horne, Abner Shimony, and Richard A. Holt. Proposed experiment to test local hidden-variable theories. *Phys. Rev. Lett.*, 23(15):880–884, Oct 1969. doi: 10.1103/PhysRevLett.23.880.

[10] Daniel Collins and Nicolas Gisin. A relevant two qubit bell inequality inequivalent to the chsh inequality. *Journal of Physics A: Mathematical and General*, 37(5):1775, 2004. URL `http://stacks.iop.org/0305-4470/37/i=5/a=021`.

[11] Daniel Collins, Nicolas Gisin, Noah Linden, Serge Massar, and Sandu Popescu. Bell inequalities for arbitrarily high-dimensional systems. *Phys. Rev. Lett.*, 88(4):040404, Jan 2002. doi: 10.1103/PhysRevLett.88.040404.

[12] A. Einstein, B. Podolsky, and N. Rosen. Can quantum-mechanical description of physical reality be considered complete? *Phys. Rev.*, 47(10): 777–780, May 1935. doi: 10.1103/PhysRev.47.777.

[13] Artur K. Ekert. Quantum cryptography based on bell's theorem. *Phys. Rev. Lett.*, 67:661–663, Aug 1991. doi: 10.1103/PhysRevLett.67.661. URL `http://link.aps.org/doi/10.1103/PhysRevLett.67.661`.

[14] Shai Emanueli and Ady Arie. Temperature-dependent dispersion equations for ktiopo4 and ktioaso4. *Appl. Opt.*, 42(33):6661–6665, Nov 2003. doi: 10.1364/AO.42.006661. URL `http://ao.osa.org/abstract.cfm?URI=ao-42-33-6661`.

[15] Alessandro Fedrizzi, Thomas Herbst, Andreas Poppe, Thomas Jennewein, and Anton Zeilinger. A wavelength-tunable fiber-coupled source of narrowband entangled photons. *Opt. Express*, 15(23):15377–15386, Nov 2007. doi: 10.1364/OE.15.015377. URL `http://www.opticsexpress.org/abstract.cfm?URI=oe-15-23-15377`.

[16] J. D. Franson. Bell inequality for position and time. *Phys. Rev. Lett.*, 62 (19):2205–2208, May 1989. doi: 10.1103/PhysRevLett.62.2205.

[17] F. Göring. *Definitionen und Sätze der diskreten Optimierung*. 2009.

[18] T.W. Hansch and B. Couillaud. Laser frequency stabilization by polarization spectroscopy of a reflecting reference cavity. *Optics Communications*, 35(3):441 – 444, 1980. ISSN 0030-4018. doi: DOI:10.1016/0030-4018(80)90069-3. URL `http://www.sciencedirect.com/science/article/pii/0030401880900693`.

[19] C. K. Hong and L. Mandel. Theory of parametric frequency down conversion of light. *Phys. Rev. A*, 31:2409–2418, Apr 1985. doi: 10.1103/PhysRevA.31.2409. URL `http://link.aps.org/doi/10.1103/PhysRevA.31.2409`.

[20] Marek Żukowski, Anton Zeilinger, and Michael A. Horne. Realizable higher-dimensional two-particle entanglements via multiport beam splitters. *Phys. Rev. A*, 55(4):2564–2579, Apr 1997. doi: 10.1103/PhysRevA.55.2564.

[21] Kiyoshi Kato and Eiko Takaoka. Sellmeier and thermo-optic dispersion formulas for ktp. *Appl. Opt.*, 41(24):5040–5044, Aug 2002. doi: 10.1364/AO.41.005040. URL `http://ao.osa.org/abstract.cfm?URI=ao-41-24-5040`.

[22] Peter L. Knight and Leslie Allen. *Concepts of quantum optics*. Pergamon Pr., Oxford u.a., 1983. ISBN 0-08-029150-3 - 0-08-029160-0. Literaturangaben.

[23] Erwin Kreyszig. *Introductory functional analysis with applications*. Wiley classics library. Wiley, New York, 1989. ISBN 0-471-50459-9 - 978-0-471-50459-7.

[24] Benjamin P. Lanyon, Marco Barbieri, Marcelo P. Almeida, Thomas Jennewein, Timothy C. Ralph, Kevin J. Resch, Geoff J. Pryde, Jeremy L. O/'Brien, Alexei Gilchrist, and Andrew G. White. Simplifying quantum logic using higher-dimensional hilbert spaces. *Nat Phys*, 5(2):134–140, February 2009. ISSN 1745-2473. URL `http://dx.doi.org/10.1038/nphys1150`.

[25] Georgios M. Nikolopoulos, Kedar S. Ranade, and Gernot Alber. Error tolerance of two-basis quantum-key-distribution protocols using qudits and two-way classical communication. *Phys. Rev. A*, 73:032325, Mar 2006. doi: 10.1103/PhysRevA.73.032325. URL `http://link.aps.org/doi/10.1103/PhysRevA.73.032325`.

[26] n.n. n.n. *n.n.*, n.n.:n.n., to be published.

[27] Markus Oberparleiter. *Effiziente Erzeugung verschränkter Photonenpaare*. PhD thesis, Ludwig-Maximilians-Universität München, August 2002.

[28] Matthew Pelton, Philip Marsden, Daniel Ljunggren, Maria Tengner, Anders Karlsson, Anna Fragemann, Carlota Canalias, and Fredrik Laurell. Bright, single-spatial-mode source of frequency non-degenerate, polarization-entangled photon pairs using periodically poled ktp. *Opt. Express*, 12(15):3573–3580, Jul 2004. doi: 10.1364/OPEX.12.003573. URL `http://www.opticsexpress.org/abstract.cfm?URI=oe-12-15-3573`.

[29] Itamar Pitowsky. *Quantum Probability – Quantum Logic*. Lecture notes in physics ; 321. Springer, Berlin / Heidelberg, 1989. ISBN 978-3-540-50679-9. doi: 10.1007/BFb0021186.

[30] Daniel Richart. *n.n.* PhD thesis, LMU, to be published.

[31] Morton H. Rubin, David N. Klyshko, Y. H. Shih, and A. V. Sergienko. Theory of two-photon entanglement in type-ii optical parametric down-conversion. *Phys. Rev. A*, 50:5122–5133, Dec 1994. doi: 10.1103/PhysRevA.50.5122. URL `http://link.aps.org/doi/10.1103/PhysRevA.50.5122`.

[32] Franco Selleri, editor. *Quantum Mechanics versus local realism : the Einstein-Podolsky-Rosen Paradox*. Physics of atoms and molecules. Plenum Pr., New York u.a., 1988. ISBN 0-306-42739-7.

[33] W. Tittel, J. Brendel, N. Gisin, and H. Zbinden. Long-distance bell-type tests using energy-time entangled photons. *Phys. Rev. A*, 59(6):4150–4163, Jun 1999. doi: 10.1103/PhysRevA.59.4150.

[34] W. Tittel, J. Brendel, H. Zbinden, and N. Gisin. Quantum cryptography using entangled photons in energy-time bell states. *Phys. Rev. Lett.*, 84:4737–4740, May 2000. doi: 10.1103/PhysRevLett.84.4737. URL `http://link.aps.org/doi/10.1103/PhysRevLett.84.4737`.

[35] Gregor Weihs, Michael Reck, Harald Weinfurter, and Anton Zeilinger. Two-photon interference in optical fiber multiports. *Phys. Rev. A*, 54:893–897, Jul 1996. doi: 10.1103/PhysRevA.54.893. URL `http://link.aps.org/doi/10.1103/PhysRevA.54.893`.

[36] Dirk Werner. *Einführung in die höhere Analysis : topologische Räume, Funktionentheorie, gewöhnliche Differentialgleichungen, Mass- und Integrationstheorie, Funktionalanalysis*. Springer-Lehrbuch. Springer, Berlin [u.a.], 2., korr. aufl. edition, 2009. ISBN 978-3-540-79599-5 - 3-540-79599-5.

[37] R. F. Werner and M. M. Wolf. All-multipartite bell-correlation inequalities for two dichotomic observables per site. *Phys. Rev. A*, 64(3):032112, Aug 2001. doi: 10.1103/PhysRevA.64.032112.

[38] A. Zeilinger. General properties of lossless beam splitters in interferometry. *Am. J. Phys.*, 49(9):882–883, 1981. ISSN 00029505. doi: DOI:10.1119/1.12387. URL `http://dx.doi.org/doi/10.1119/1.12387`.

Danksagung

An dieser Stelle möchte ich all den Menschen danken, ohne die die Fertigstellung dieser Arbeit nie möglich gewesen wäre.

Allen voran möchte ich Harald Weinfurter für seine Unterstützung und dafür danken, dass er es mir ermöglichte, in seiner Arbeitsgruppe meinen Interessen nachzugehen.

Besonders herzlich danken möchte ich auch Daniel Richart, der mich mit dem Experiment vertraut gemacht hat und stets zwei offene Ohren für mich hatte. Die Arbeit in unserem kleinen Team hat mir große Freude bereitet!

Auch den übrigen Gruppenmitgliedern, besonders den "Garchingern" Christian Schwemmer, Roland Krischek und Alexander Niggebaum möchte ich für die offenen Diskussionen über jegliches Thema und für die Hilfe in Rat und Tat danken.

Vielen Dank auch an meine Familie für die großartige Unterstützung!

Erklärung

Mit der Abgabe dieser Diplomarbeit versichere ich, dass ich die Arbeit selbstständig verfasst und keine anderen als die angegebenen Quellen und Hilfsmittel verwendet habe.

München, den 30. September 2011

Yvo Fischer